DISSERTATIONES PHYSICAE UNIVERSITATIS TARTUENSIS

42

LOW CURRENT MODE
OF NEGATIVE CORONA

VILLU REPÄN

The study was carried out at the Institute of Experimental Physics and Technology, University of Tartu.

The dissertation was admitted on January 29, 2004, in partial fulfilment of the requirements for the degree of Doctor of Philosophy in physics (optics and spectroscopy), and allowed for defence by the Council of the Department of Physics, University of Tartu.

Supervisor: Dr. Matti Laan, Institute of Experimental Physics and
                Technology, University of Tartu, Estonia

Opponents: D.Sc. Yuri Akishev, Troitsk Institute for Innovation and
                Fusion Research, Russia

                D.Sc. Henn Käämbre, Institute of Physics,
                University of Tartu, Estonia

Defence: April 8, 2004 at the University of Tartu, Estonia

CONTENTS

LIST OF ORIGINAL PUBLICATIONS

I. Laan M, Paris P, Repän V 1997 Triggering of Negative Corona *Inv. Pap. XXIII ICPIG* (Toulouse, France) *Journal de Physique IV* 7 Col. **C4,** 259–270

II. Repän V, Laan M, Paris P, Aarik J, Sammelselg V 1999 Negative Coronas: Low Current Mode — Pulse Mode Transition *Czech. J. Phys.* **49** 217–224

III. Laan M, Aarik J, Josepson R, Repän V 2003 Low Current Mode of Negative Corona: Mechanism of Electron Emission *J. Phys. D: Appl. Phys.* **36** 2667–2672

IV. Repän V, Laan M and Plank T 2002 Electric field modeling for point-plane gap *HAKONE VIII: Int. Symp. High Pressure Low Temperature Plasma Chemistry* (Tartu, Estonia) *Contrib. Papers* **P2.2** 134–138

V. Repän V, Laan M, Paris P 1999 Transition to Trichel pulses for Cathodes of Different Photoelectric Yields *Proc. XXIV ICPIG'99* (Warzaw, Poland) *Contrib. Pap.* Vol. **II** P-218 175–176

VI. Laan M, Repän V, Paris P 1998 Waveforms of UV-induced current pulses of negative corona *Contrib. Papers of 11th Symp. on Elementary Processes and Chemical Reactions in Low Temperature Plasma* (Low Tatras) **2** 271–273

VII. Laan M, Paris P, Repän V 1997 Gas flow contra stagnant medium: changes of cathode emissivity in a point-plane gap *ESCAMPIG 13* (Poprad, Slovakia, 1996) Part B **20E** 431–432

VIII. Repän V 1996 Negatiivse koroona tekkemehhanismi uurimine *Magistritöö* Tartu 47 lk.

IX. Laan M, Repän V, Roos H 1994 Repetition rate of Trichel pulses and conditioning *10th Symp. on Elementary Processes and Chemical Reactions in Low Temperature Plasma* (Slovakia, High Tatras) *Acta Physica Universitatis Comenianae* **35** 175–179

X. Laan M, Paris P, Repän V, Uustare T 1994 Laser-triggered negative corona *12th ESCAMPIG* (Noordwijkerhout, The Netherlands) *Inv. Lectures and Contr. Papers* 358–359

First three CC level publications are parts of the thesis.

Comment on participation

The experimental part of the study is totally carried by V. Repän. He also played a major role in modelling.

1. INTRODUCTION

Corona discharges, i.e. gas discharges in highly divergent electric field, belong to the sphere of thermodynamically non-equilibrium and non-stationary low temperature plasma. This kind of plasma is unstable, small fluctuations of electron density or their temperature may cause huge quantitative and qualitative changes. Thus for example at near-atmospheric pressures in negative corona the current may grow by nine orders of magnitude during few nanoseconds.

Processes taking place near the electrodes often determine the reasons for the development of ionisation instabilities. Generally the study of near-electrode instabilities at high pressures is complicated, as the events are badly localised in space and the feedback from the side of the discharge plasma overshadows the processes studied. In the case of corona discharges the discharge events are much better localised and the influence of the discharge plasma is considerably suppressed. Besides, as it has been proved in many studies, in its initial stage the feature of ionisation instabilities depends only weakly on discharge gap geometry. Thus we may conclude that the results of corona studies highlight also a much wider area in plasma physics.

During last two decades a considerable progress has been achieved in understanding the corona processes. First, nowadays experimental technique allows to record discharge characteristics with adequate time resolution. Secondly, a number of fast algorithms have been worked out for discharge modelling. The discharge mechanism is clarified solving a set of hydrodynamic equations. The results of the modelling are compared with the experiment and it seems that in all cases at least a satisfactory coincidence is achieved for the discharge stage where the discharge current is easily measurable. The problem is that the coincidence is achieved in spite of very different assumptions about the emission mechanism of first electrons. Consequently, only experiment could answer to the question which model is favoured. At the same time the information about the earlier discharge stage is rather poor.

On the foreground of the present study there is the experimental investigation of the discharge stage preceding the fast rise of the current. The aim of the thesis is to find out the model of emission and to compare the results of the model with experimental findings.

The paper has the following structure. Chapter 2 gives an overview of main parameters characterising the negative corona discharges and the basis of computer models. The description of computer models includes also the author's comments. Further follows the description of the previous attempts of the external triggering of the negative corona and the results concerning the low current mode of the discharge. Mechanisms of electron emission, which assume the participation non-metallic inclusion at the electrode, are presented in more

detail. The final section contains the problems to be solved in order to achieve the aim of the paper.

Chapter 3 gives the experimental setup and means used for the triggering and detection of discharge parameters.

Chapter 4 is dedicated to the electric field modelling and calculation of basic data (like ionisation integral, etc) characteristic to the used discharge gap. This chapter also involves the calculation of the current components of the avalanche developing in the discharge gap.

Chapters 5, 6 collect the experimental results of the study. Besides, the final section of Chapter 5 presents the calculations that allow to estimate the limit, whence the space charge of negative ions plays an important role.

Chapter 7 brings out the model of emission. The validity of the model is tested by the comparison of the model conclusions with experimental findings. The chapter ends with the list of open problems and proposals for further studies.

Summary both in English and Estonian, presents the most important results from the author's viewpoint.

2. BACKGROUND

2.1. Definitions

According to [1]: a corona is a self-sustained electrical discharge where the Laplacian (geometrically determined) electric field confines the primary ionization processes to the regions close to high-field electrodes.

Corona is called unipolar if the high-field region exists only near one of the electrodes (active electrode). When DC voltage is applied to the discharge gap and the high-field region is concentrated near the electrode of negative polarity we speak about negative corona. The limited volume where the ionization takes place is the ionization zone. The other part of the discharge gap is called the drift zone. The favorite geometry of the discharge gap used in corona studies is the point-plane geometry.

The basic data and results of negative corona studies till 1980s are collected in [1, 2, 3]. The following overview describes the main regularities typical for unipolar negative corona at pressures >10 kPa. As the gas medium and/or the discharge gap geometry used in different studies differ considerably, the numerical data have only an illustrative character.

2.2. Negative corona in different gases, Trichel pulses

The appearance of the corona discharge in electropositive gases was first described in [4]. The observations were made in point-plane gap for discharges in H_2, N_2 and Ar. In nitrogen two steady modes of the discharge were fixed. At low currents only a faint and diffuse light was detected near the point while at high currents the discharge contracts to the concentrated form. Similar studies but in purer conditions were described in [5] where besides the description of the discharge appearance also the current-voltage characteristic was presented.

A more detailed study of the LCM in a point-plane gap and in pure nitrogen at atmospheric pressure was carried out in [6]. Current-voltage characteristic was recorded for two steady modes of a huge current difference (Figure 1). At a certain voltage there occurs a spontaneous and fast transition from the mode of the lower current to that of the higher current. We named the modes the high current mode (HCM, region CEF in Figure 1) and the low current mode (LCM, part AB in Figure 1) of negative corona [7 (**Paper I**)]. Current pulse corresponds to LCM-HCM transition and its peak value for experimental conditions like during the recording of the dependence in Figure 1 is ~10^{-2} A.
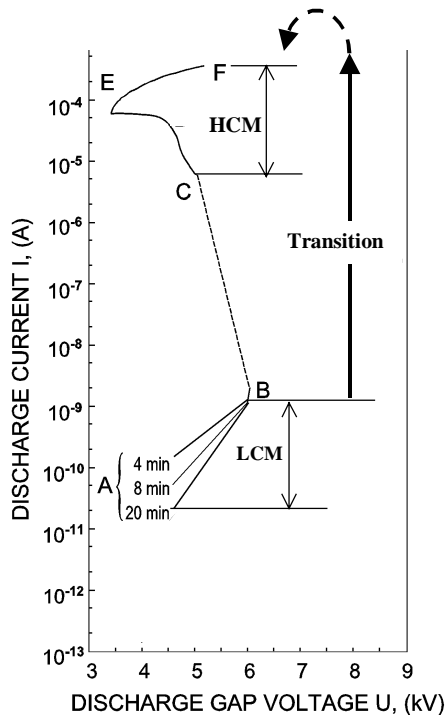
Figure 1. Current-voltage curve in pure nitrogen at atmospheric pressure; [6].

Usually, speaking about negative corona discharge the processes occuring during LCM-HCM transition and/or HCM mode are referred to.

In electropositive gases the high-current mode, HCM, is controlled by the current-limiting resistor and the capacitance in the power feed. Figure 2 reflects the establishment of HCM occurring after LCM-HCM transition. In this case the voltage drop at the discharge gap did not remain constant and in the gas with 0% of oxygen and for $t > 5\,\mu$ s the current decrease was caused by the decay of the voltage drop. Addition of oxygen shortens the decay time of the current pulse as well as the steady value of HCM current. Starting from a certain oxygen concentration the steady form of HCM is missing and only a current pulse is recorded. This pulse is known as Trichel pulse after G. W. Trichel who first described the phenomena of negative corona [9]. A pulsed form of the negative corona is typical for gases containing electronegative components.

11
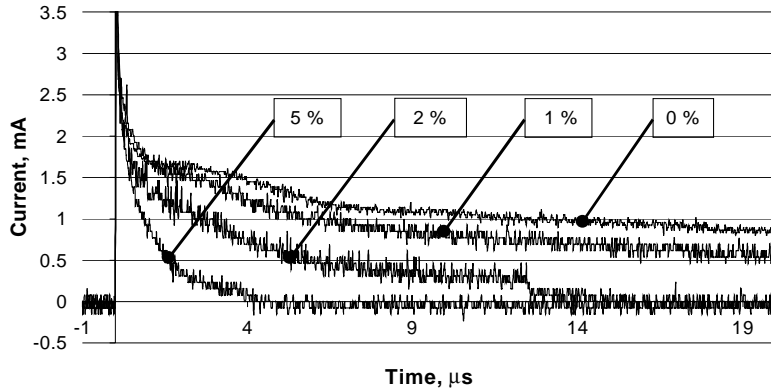
Figure 2. Trailing part of the current of LCM-HCM transition in N_2+O_2 mixtures at atmospheric pressure; labels indicate the concentration of oxygen; [8].

At a fixed voltage a number of Trichel pulses arises. Very close to the onset potential Trichel pulses follow each other in a random manner. Further growth of the voltage leads to the establishment of a highly regular train of pulses (Figure 3A) characterised by the repetition rate, RR (s^{-1}). Starting from the pioneering studies [9] the regularity of pulses was linked with the space charge of negative ions moving in the drift zone. The space charge field created by the previous Trichel pulse reduces the total field near the point thus breaking the rise of the next pulse. [11] given a model of the phenomenon. Numerical estimations show that the time interval between the pulses (i.e. reciprocal of the repetition rate) is considerably shorter than the drift time of negative ions in the gap. It means that a lowering of the field near the point is the effect of the accumulation of numerous clouds of negative ions from the previous Trichel pulses. Later it was found [10], that the first Trichel pulse rising has a considerably larger amplitude than the following ones and a regular train establishes after some tens of pulses. The modelling carried out in [12], proved the assumption that the space charge of negative ions accumulated in the gap controls the repetition rate of Trichel pulses. Besides, the model describes properly the pulse sequence presented in Figure 3B and a good agreement between the calculated and measured repetition rates was achieved [13].

12
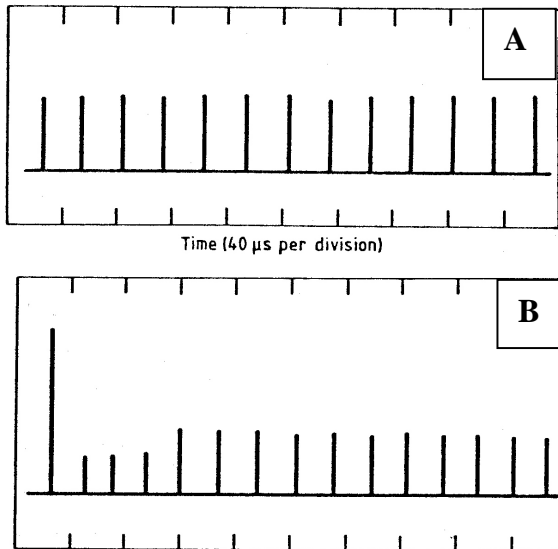
**Figure 3.** Train of Trichel pulses in oxygen; A — regular train; B — 15 first pulses; [10].

2.3. Leading edge of Trichel pulses

The regularities at the trailing edge of Trichel pulse are clearly related with the attachment coefficient and concentration of the electronegative component. The situation at the leading edge is more complicated. At atmospheric pressure the current growth by more than six orders of magnitude takes place during few nanoseconds. Such a short rise-time overruled attempts to explain the current growth by the development of successive avalanches [2]. The assumption that during the current rise many avalanches develop in parallel gives a much better prediction of the fast current rise [14]. This viewpoint was embodied in the computer model of the first Trichel pulse [15]. In one-dimensional model a set of continuity equation for electrons, positive and negative ions, was coupled with Poisson's equation. The equations included ionization, attachment, recombination, and electron diffusion. It was the first study that gave insight to the detailed mechanisms of the pulse development.

Two important details of the described model should be pointed out. First, it was set that secondary electrons ensuring the self-sustained discharge, are liberated by photons i.e. γ_{ph} feedback mechanism was assumed. Secondly, the calculation was initiated by the release of 400 seed electrons.

13

The model gave a physical background of Trichel pulse and the computed current was very similar to that measured in oxygen. However, the calculated waveform of the current at its rising part does not coincide with those recorded in many experiments. A complicated structure of the current rise was first recorded in [16]: there was a step at the leading edge. Later a number of studies followed, where also the step (Figure 4) was recorded. The finding of the step forced to modify the model presented in [15]. Its new version [18] explains the step in terms of independent photon (γ_{ph}) and ion (γ_i) feedback mechanisms.

Both photons and ions causing the feedback are created at the same moment but the ions reach the point later. Thus the photons are responsible for the rise of the step and the ions cause the main rise of the current. The experiment, [10], specially carried out for the verification of the model, seemed to prove the assumptions.
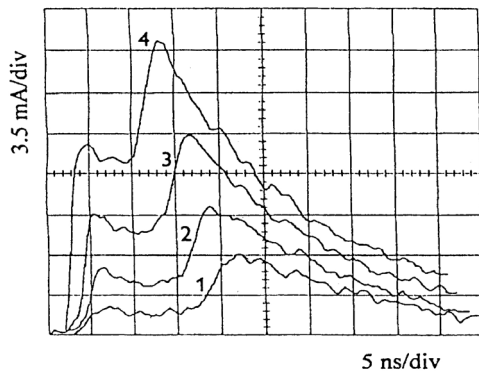
Figure 4. Leading edge of Trichel pulse in oxygen; larger numbers of curves indicate higher voltages; [17].

It should be pointed that the value $\gamma_{ph} = 2 \times 10^{-4}$ used in [18], is close to the literature data [19], while the value $\gamma_i = 0.12$ for near-atmospheric pressures and molecular gases seems to be too high.

A large cycle of measurements [17, 20–24] was dedicated to the study of the leading edge of the first Trichel pulse. The regularities of the step were recorded for different gas mixtures as a function of overvoltage. The conclusion of the authors was that the step is controlled by the photoemission feedback but in contrast with [18], the main peak of the current pulse reflects the development of the cathode-directed streamer-like ionization wave. The last mentioned experiments also found the dependence of the current waveform on the point coating: adding the CuI layer to the Cu point made the step more pronounced.

14

The dependence of the current waveform on the point material and/or coating is also fixed in [10, 25, 26].

In the computer model [12] a similar set of continuity equations like in [15] was the basis of the calculations. The most important difference was that the model considers only the ion feedback and calculations were made for $\gamma_i = 10^{-2}$. The analyses showed the reality of the cathode-directed ionisation wave connected with the movement of the high-field ion-caused region. In the current pulse the movement of the ionisation wave appears as the step and the peak of the current corresponds to the moment when the cloud of positive ions reaches the point. Authors stated a reasonable agreement with the experimental results.

It should be pointed that the ionisation wave of the latter model and the wave assumed in [17] are responsible for different parts of the current pulse. Besides, as the properties of the ionisation wave should depend mainly on the gas medium and voltage applied, it is difficult to explain the dependence of the current waveform on the material of the point electrode.

The next model, [27], supposes that the ion-impact is the secondary emission and initially was set $\gamma_i = 0.5$. Like in [15] the calculation started with 400 initial electrons. It was concluded that the brake of the initial current growth is caused by the build-up of the plasma plume with a low value of the field strength. For this reason the slope of the current growth reduces i.e. the step appears. When the build-up of the plasma plume is complete, in its cathode-side edge exits a high-field region. The growth of the ionisation rate in this region causes the appearance of the current peak.

The advantage of the latter model is that the authors tested the influence of different values of γ on the discharge current. The value $\gamma_i = 0.12$ gave the rise-time 10 ns, which is considerably longer than that recorded in experiments at atmospheric pressures.

In [28, 29] it was supposed that the regularities on the leading edge could be explained by the field emission. As the Laplacian field strength is considerably lower than that needed for efficient Fowler-Nordheim type of emission a field enhancement factor β was introduced. β was given values close to those, usually used in the case of polished cathode surfaces. The best fit of the calculated current waveform to the experimental one was achieved assuming that the factor is time dependent i.e. $\beta = \beta_0 + \beta(t)$. The growth of the enhancement factor was linked with the formation of the cathode sheath. It is remarkable that when the coefficient of the ion-caused feedback was artificially set to zero, the current waveform did not change.

15

2.4. Triggering of Trichel pulses and LCM

2.4.1. Onset potential

Computer models [12, 15] connect the rise of Trichel pulses with Townsend condition of the self-sustained discharge $\gamma \exp\left(\int \alpha_{eff} dx\right) = 1$, where α_{eff} includes both ionization and attachment coefficients. In the case of low-pressure discharges in homogeneous field the coefficient γ depends on the cathode material and it is possible to distinguish discharges ruled by ion and photon feedback mechanisms [30]. In contrast, already in [31] it was found that Trichel pulse onset does not depend on point material but it depends considerably on the point history. An explanation of the effect was that at atmospheric pressures the electron emission ability is determined by the gas absorbed at the surface and not by the substrate material [3]. A little later it was found [3] that below the onset potential of Trichel pulses there exists a self-sustained discharge of a very low current value. This finding forced to conclude that Trichel pulse onset does not mark the onset of the self-sustained discharge.

2.4.2. Triggering methods

In order to determine properly the onset potential of Trichel pulse as well as to clarify the reasons of its rise, different methods of external triggering were used.

Attempts to use radioactive β/γ sources for triggering were not successful, as the probability of the creation of the triggering electrons in a very limited volume near the point is low [3]. For this reason it was impossible to separate initiated Trichel pulses from those rising spontaneously.

The triggering by UV light from mercury lamp was sometimes lowering, sometimes raising the value of the threshold potential. High intensities of UV light suppressed Trichel pulses and a satisfactory triggering was achieved at low values of the intensity [32]. Besides, a correlation was found between the efficiency of UV triggering and the conditions at the point surface. The presence of non-metallic specks at the point decreased the efficiency of UV triggering.

A regular train of Trichel pulses was observed when the point surface was covered with layers of non-metallic materials like MgO and Al_2O_3. This result was explained by Malter effect i.e. the charging of insulating layers by positive ions [3]. When the field across a charged insulating layer reaches field emitting proportions, the emission of electrons occurs. [33] also tested the dependence of insulating coatings on Trichel pulse rise. Soft X-ray pulses were used for triggering. A thin layer of the transformer oil shifted the onset of the spontaneous (i.e. non-triggered) Trichel pulses to considerably higher voltages but X-ray triggered pulses rise at the same voltage like in the case of non-coated

points. At higher voltages X-ray pulse initiates a number of Trichel pulses. The results seem to prove the importance of Malter effect.

The effect of the point heating was first described in [34]. A small rise of temperature turned the train of Trichel pulses irregular but when the heated point started to emit in the visible region a regular pulse sequence was restored. As the temperature became higher the repetition rate increased. Such behaviour was explained by the changes of gas density near the point electrode. The role of the point temperature was also studied in [35]. The current pulses were triggered by XeCl (λ = 308 nm) laser, changing both the irradiance at the point surface and the voltage applied. The current peak was a function of irradiance and voltage, and at a fixed value of irradiance the peak depended on voltage like it is typical for thermoionic field-assisted emission. In [36], where Trichel pulses were triggered by the radiation of XeCl lamp, the influence of the point temperature was also tested. For this purpose the infrared radiation was directed to the point surface and more than 2-fold growth of the repetition rate was recorded. As the experiments were carried out in airflow the changes of the gas density played a minor role.

2.4.3. Low current mode (LCM)

Already the first studies of negative corona described the discharge phenomena existing below the onset of Trichel pulses. The prepulses found were associated with a faint glow near the point [3]. In the case of γ-ray triggering [32] the mean current was less than 10^{-12} A, but the size of the current kicks exceeded this value by several orders of magnitude. The appearance of the pulses was irregular and their size grows with the voltage increase. At the same time before the onset of Trichel pulses the mean current induced by UV, reached the value of 10^{-8} A.

In [37] the characteristics of the discharge induced by β-ray and UV radiations were recorded. The values of the mean current in both cases were close and changed with voltage from 10^{-10} A to 10^{-7} A, while the amplitude value of the current pulses was 10^{-6} A. The oil or $Ca(OH)_2$ coatings caused a growth of both the mean current and the amplitude of the pulses. Current pulses arising at voltages below the onset of Trichel pulses are also described in [38]. The pulses had a small (< 400 nA) amplitude and at lower voltages their train was irregular. Near the onset the pulses appeared more regular and their amplitude increased. The results of the study of the statistical properties of Trichel pulses at AC voltages are presented in [39]. The appearance of the pulses called quasi-Trichel pulses, was connected with Malter effect. The explanation was that the pulses appear when the intensity of Malter emission is not sufficient for Trichel pulses. Pulses, preceding Trichel pulse were fixed in [24] with considerably higher time resolution than in aforementioned studies. In

CO_2 the pulses have an amplitude $< 10^{-4}$ A and they may transit to Trichel pulses.

The regularities of the mean current of LCM in nitrogen are described in [33, 40]. In both cases the discharge was a self-sustained one. By appearance, LCM of discharge was a very faint diffuse light near the tip of the point electrode. The current-voltage characteristic of the discharge is time-dependent (Figure 1, region AB): according to [33] after a voltage increment the value of a new current value diminishes with time. The establishment of a constant current value takes tens of minutes. At voltages very close to LCM-HCM transition the current stagnation is replaced by an increase, ending with the transition. As the current-voltage dependence for a certain time moment was linear in Fowler-Nordheim plot, the authors supposed that the discharge of LCM is determined by the field emission. In [40] it was found that it is possible to record the current of LCM only in the case of the used gas, after a new filling of the discharge chamber the current was not detectable. The effect was explained by the desorption of electronegative impurities, which modify the discharge.

2.5. Emission mechanisms

2.5.1. Deviation from Paschen's law

From the condition of the self-sustained discharge $\gamma \exp\left(\int \alpha_{eff}\,dx\right) = 1$ it is possible to derive the relationship named Paschen's law [41]

$$U_{onset} = f(Nd),$$

where U_{onset} is the voltage at the threshold of the self-sustained discharge, N is gas density and d is electrode separation. The validity of the relationship is experimentally controlled for DC, AC and even for microwave discharges [42] in a very wide range of conditions, and it holds. Remarkable departures from Paschen's law appear only at near-atmospheric pressures and for fields $> 10^5$ V/cm. It should be pointed that the latter value is close to the field strength at the point surface at the threshold of negative corona.

In [43] the departure from Paschen's law was explained by the field emission. The emission starts from small irregularities at the cathode surface where the field strength achieves the value 10^7 Vcm^{-1}. The space charge of the positive ions created increases the field, thus causing a steep rise of the current. For quantitative treatment the effective feedback coefficient γ was defined as the ratio of the field-emission electron current density to the incoming positive-ion current density. The new criterion of the self-sustained discharge was in agreement with the experiment.

In [44, 45, 46] another explanation of the role of the field emission was presented. The emission current at the protrusion tip on the cathode causes the

heating of the protrusion and finally it explodes. As a result a burst of electrons is emitted, giving a start to the breakdown. Several experimental results prove the validity of the model.

Three independent parameters are needed for the proper description of the emission from the protrusion: the field enhancement factor, the size of the emitting area and the work function of the electrode material. Experiments allow determining only their combinations. The main problem is that setting reasonable values of the enhancement factor and the work function lead to very small values of the emitting area [44]. To overcome the difficulties it is assumed that other factors, like foreign inclusion and gas absorption at the electrode surface influence the emission [45].

There is much in common in the initial stages of the discharge in vacuum and high-pressure gases [45, 46, 47]. In both cases the values of the field strength at the cathode surface are close, current follows Fowler-Nordheim (FN) type of emission and emissive sites on electrodes in vacuum and gases are spatially correlated. At the same time in vacuum the situation is less complicated and the regularities of the emission mechanism appear more clearly. For this reason in the next two subsections are presented the models of the electron emission in vacuum.

2.5.2. Dielectric switching mechanism of emission

The road passed in the developing of the mechanism is described in [48–50]. Experiments show that the vacuum breakdown starts at fields, which are two orders of magnitude lower from the value needed for effective FN emission from metal. At the same time the recorded field enhancement factor at emissive sites was < 10. The next result was that the emission site has insulating properties. On the basis of these findings was developed a quantitative model of electron emission of metal-insulator-vacuum (MIV) structure.

Figure 5 reflects the main steps of the switch-on an emissive site at the cathode surface, taking place in the increasing electric field. The applied field causes a bending of bands and the structure of MIV bands transforms (Figure 5A, 5B). Figure 5B presents the situation when the electrons start to tunnel trough the metal-insulator barrier. These electrons fill the traps existing below the bottom of the conduction band, Fermi level shifts towards the conductive band and the height of insulator-vacuum barrier decreases. When the traps are filled, the next electrons fill the surface states. As a result the field of electrons at the surface states screen the bulk of the insulator from the external field and it cuts the tunnelling from the metal (Figure 5C). The next increments in the applied field lead to a situation, where electrons can again penetrate the metal-insulator barrier (Figure 5D). Besides, because of lowering the thickness/ height of the insulator-vacuum barrier (Schottky effect) electrons are able to penetrate and/or overcome the barrier i.e. the emission starts. Experiments

verify that in the spectrum of the emitted electrons exist both thermoionic and tunnelling components.
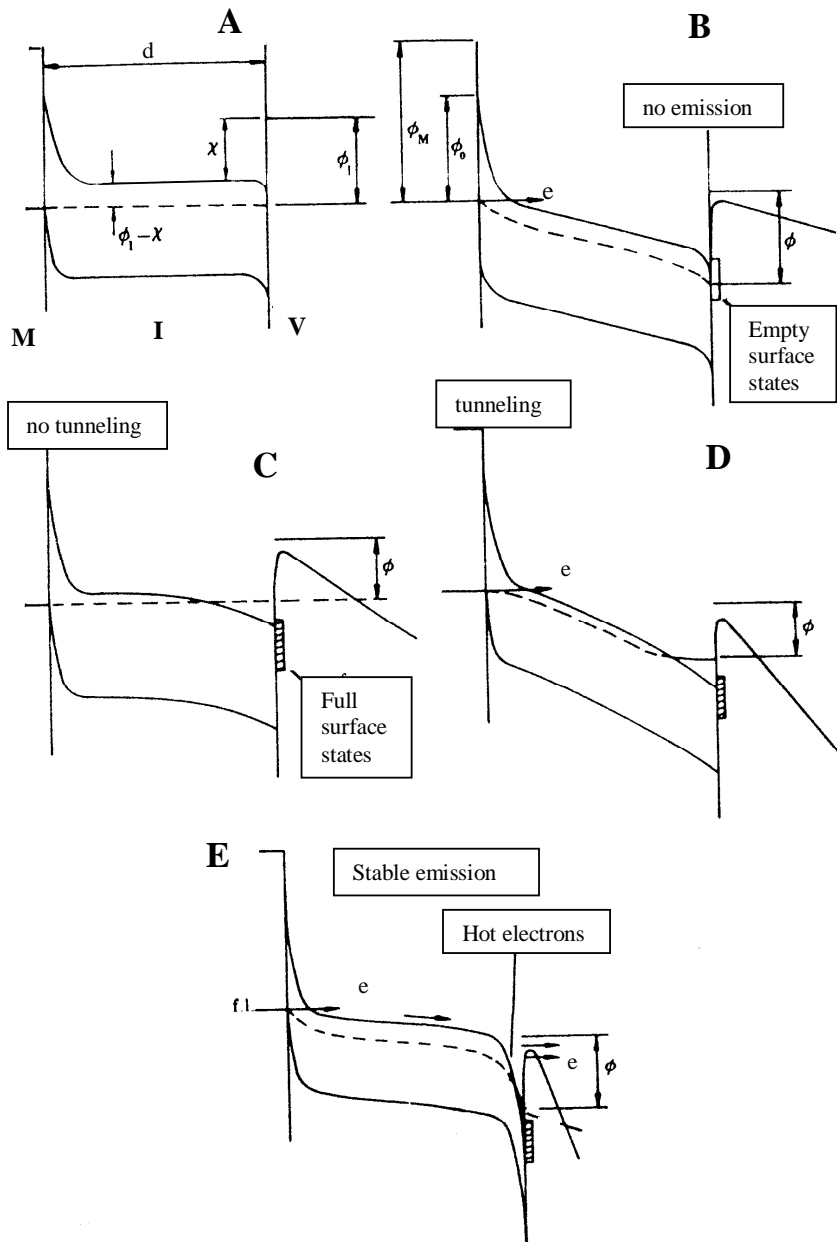

Figure 5. Emission mechanism of metal-insulator-vacuum (MIV) structure.

2.5.3. Emission from electrodes coated with thin layers

Recently have appeared publications, [51–53], dealing with the experimental and theoretical study of MIV structures. In these studies the thickness of the insulating layer had the order of the magnitude of 10 nm. The coatings permit an efficient emission at electric fields, which are 10^2–10^3 times lower than in the conventional case. The current-voltage curve has three characteristic regions. The first one fits with that of FN type of emission. The second one is specific of an emission of electrons through and over the insulator-vacuum barrier, which has been lowered due to Schottky effect. At still higher fields very rapid, explosive like, growth of electron emission is observed. There is a remarkably strong dependence on the temperature: the increase of the temperature from $20\ ^0$C to $100\ ^0$C causes the current growth almost five times.

Figure 6 presents the calculated energy-band diagram evolution during the growth of the applied field, the field increases from 5×10^4 to $1.4\times10^5\ \text{Vcm}^{-1}$ [53]. The evolution has two characteristic steps. During the first step (electron injection) the electrons penetrating the metal-insulator barrier are accumulated near the insulator-vacuum interface. The space charge of electrons causes the bending of bands. Substeps a, b, c, in Figure 6 correspond to the different values of the accumulated space charge. During the next step the band structure inside the insulator remains almost unchanged but the height and thickness of the insulator-vacuum barrier is lowering with the growth of the applied field. The spectrum of the emitted electrons has the thermoionic and tunnelling components. In the last stage of emission dominates the thermoionic component.
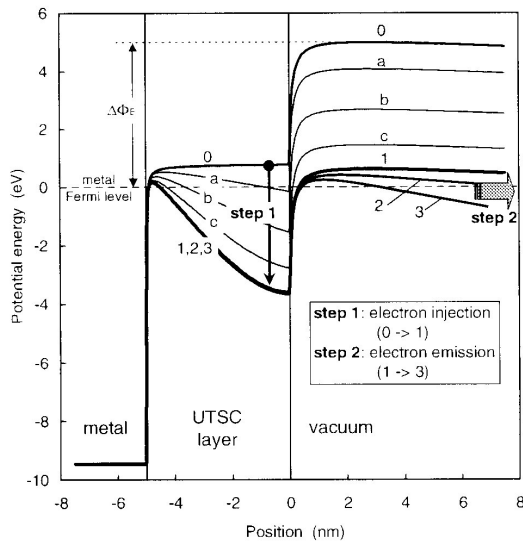
Figure 6. Steps of electron emission for thin dielectric coatings; [51].

2.6. Conclusions and research program

As it follows from the overview, nowadays knowledge about the negative corona allows a satisfactory explanation of processes taking place during the current decay. The same conclusion is valid in the case of the repetition rate of Trichel pulses.

The hydrodynamic approach is used in all computer models of Trichel pulse. The data, like ionization and attachment coefficients, etc do not differ much, but considerably different electron emission mechanisms are supposed. The most amazing is that all models give satisfactory coincidence between the calculations and experiment. Consequently, only on the basis of the information extracted from the models it is impossible to make reliable conclusions about the mechanism of Trichel pulse rise.

The information about the low current mode of the discharge is rather poor. It seems that the mode has two components, the steady and the pulsed one but the relationship between them as well as their role in the Trichel pulse formation remains open.

It seems that the models assuming FN type of emission work in the case of gas discharges at high values of the reduced field i.e. in the short discharge gaps and/ or at values of the voltage, which considerably exceed the onset voltage. If the model is working also in the case of corona discharge near its inception voltage, is not clear.

Experiments showed that the rise of Trichel pulse is related with non-metallic inclusions at the cathode. The problem is that the surface-gas interface is a very complicated physical system and such important parameters like nature and thickness of inclusions are not known or they change because of plasma-surface interaction.

We assume that the clarifying of the mechanism of LCM should give better understanding of processes responsible for the rise of Trichel pulses. The task of the study could be achieved if

- The temperature, humidity and pressure of the gas medium are controlled or fixed, the medium is dust free.
- The non-metallic coatings have controlled composition and thickness and a sufficiently long life time.
- Reliable triggering methods of the discharge are elaborated.
- The dependence of the discharge characteristics as a function of triggering, coating type, and applied voltage is recorded with a sufficient time resolution.
- The electric field distribution in the discharge gap is modelled.
- On the basis of the field distribution the basic data like ionisation integral, drift times of charge carrier etc are calculated for the discharge gap used.
- The model of emission should be drawn.
- Conclusions from the model should be compared with the experimental results.

3. EXPERIMENTAL SETUP

3.1. Discharge chamber

Figure 7 presents the main parts of the experimental device.
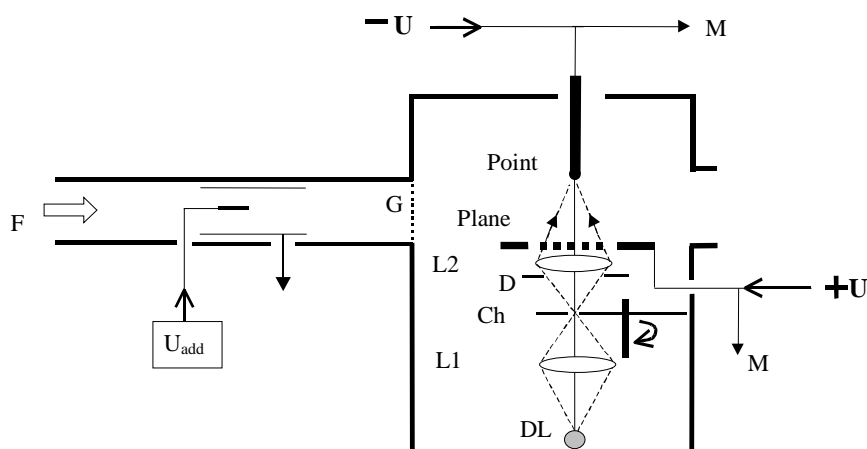
Figure 7. Sketch of the experimental device; F — dustfree airflow; U — power supply; U_{add} — power supply for additional corona; G — set of grids; DL — deuterium lamp; L1, L2 — lenses; Ch — rotating chopper; D — diaphragm; M — measuring circuits.

The experiments were carried out in an aluminium chamber of cross-section 20×20 cm^2. The point-plane discharge gap has spacing 4 cm. The plane electrode was an aluminium plate of 15 cm diameter. In its centre there was an aperture of 5 cm diameter covered with a stainless steel grid of mesh size 2 mm.

The power supply allowed to change the voltage with a smallest step of 10 V. In different experiments either point or plane electrodes were stressed.

3.2. Point electrodes

The point electrodes were 10 mm long wires of 1 mm diameter with a hemispherical tip. In total more than fifty point electrodes made of platinum (Pt), molybdenum (Mo) and copper (Cu) were used. Firstly the points were mechanically polished. Their curvature radius differed from 0.5 mm not more than 10 μm and under 100-fold magnification their surface seemed to be smooth. After mechanical treatment all points were cleaned in an ultrasonic bath using petrol, acetone and tridestilled water. Before and between experiments, electrodes were kept in dried helium medium.

23

Both point electrodes without special coatings and the ones with non-metallic coatings of controlled composition and thickness were used. Table 1 gives the list of the point types used.

The electrodes with TiO_2 and HfO_2 films were prepared using atomic layer deposition method [54, 55]. Deposition temperature as low as 100 °C was chosen in order to obtain the coatings of minimum surface roughness. The films grown in this way were amorphous. TiO_2 films have the optical band gap of 3.3 eV [56] and according to the literature data [57] the HfO_2 films have the optical band gap > 5.5 eV.

Table 1

	Substrate	Coating	Procedure
1	Cu	fresh	washed in distilled water or ethanol
2	Cu	aged	case 1 + 24 h
3	Cu	oxidized	case 1 + heating (150° C, 1 h)
4	Cu	CuI	soaking in solution of 1 g/l iodine in acetone for 5 min [17]
5	Cu	3 & 70 nm of HfO_2	atomic epitaxy [54, 55]
6	Cu	3 & 100 nm of TiO_2	atomic epitaxy ($TiCl_4/H_2O$, 100° C, 1 nm = 10 cycles) [54, 55]
7	Cu	C	spraying surface with Graphit 33 [17]
8	Cu	ion bombardment	glow discharge in Ar at 10 kPa running for 5 min [17]
9	Mo	fresh	like in case 1
10	Mo	aged	like in case 2
11	Mo	3 & 70 nm of HfO_2	like in case 5
12	Mo	1, 3, 70 & 100 nm of TiO_2	like in case 6
13	Pt	fresh	washed in distilled water or ethanol
14	Pt	aged	natural
15	Pt	C	like case 7
16	Pt	ion bombardment	like case 8

At least two samples of every point type were used. Because of the discharge-surface interaction the discharge characteristics changed with time.
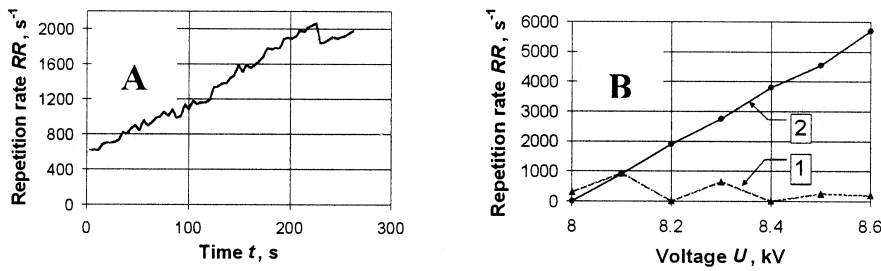
Figure 8. Oxidized Cu point; stressed point; A — repetition rate as a function of time, U = 8.2 kV; B — repetition rate as a function of voltage, 1 — virgin point, 2 — used point.

In [58] we recorded the repetition rate of Trichel pulses as a function of time. Figure 8A presents the temporal change for a virgin point at a fixed voltage: the repetition rate increases gradually with time. Furthermore, for virgin points the dependence on voltage was missing (Figure 8B). Both dependencies in Figure 8B were recorded in a similar manner: firstly the voltage was increased by 0.2 kV step ($8.0 \rightarrow 8.2 \rightarrow$ etc) and then decreased ($\rightarrow 8.5 \rightarrow 8.3 \rightarrow$). After a 20h break (used point) the repetition rate depended on voltage almost linearly. Described temporal changes were more pronounced in the case of thick layers, like 100 nm of TiO_2, and were practically missing for thin layers.

As it was fixed by scanning electron microscope, at the surface of the points appeared craters of diameter 1 μ m. It is remarkable that even for points without special coatings in the sites of craters the traces of non-metallic inclusions were always detected (Figure 9).

To reduce the influence of the morphological changes the study of Trichel pulses was made in a comparatively narrow range on voltages where the repetition rate was less than $10^4 \, s^{-1}$. In this case a good long-term reproducibility of results was achieved. LCM of the discharge did not cause any remarkable changes at the point surface.

3.3. Medium

According to the experiments and modeling, the presence of solid and liquid particles could considerably change the discharge parameters [60, 61]. At the same time the negative corona originates a number of chemical reactions and it is a source of fine dust particles [62, 63]. Finally, atoms/molecules in metastable states, created by corona, could extract electrons from the cathode. Accumu-

25

lation of all these particles in the discharge gap may lead to changes in the discharge parameters. For this reason the experiments were carried out in a dust-free airflow.
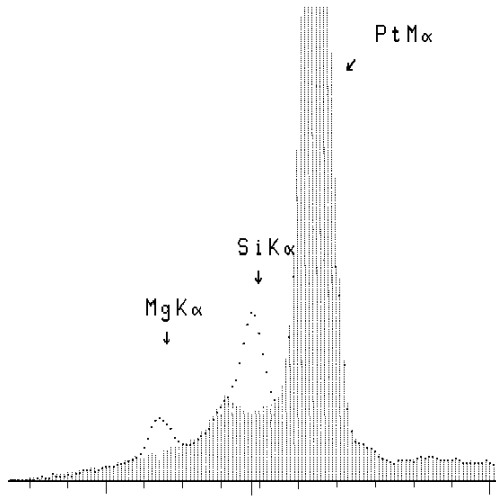
Figure 9. X-ray spectra of Pt point. Shadowed area — spectrum of a site at the point surface, which is not influenced by Trichel pulses; the peaks of foreign inclusions are recorded at the position of a crater [59 (paper **II**)].

The rate of the airflow entering the discharge chamber, was changed from 0 to 9 ms^{-1}. Dust and ions in the entering ambient air were removed. A high-efficiency fibre filter was used: only particles of less than 10 nm in diameter were recorded by an aerosol spectrometer [64] and their concentration was $< 10^3$ cm^{-3} [65]. With the help of a heat exchanger it was possible to fix the temperature in the limits 15–30°C. The air pressure p changed within the limits 741–772 Torr. The value of the relative humidity was set using a droplet-free humidifier [65]. The temperature, relative humidity and pressure were recorded. Voltages U_e recorded in the experiment were reduced to the standard conditions ($p_0 = 760$ Torr and $T_0 = 293$ K) according to the relationship $U = U_e p_0 T / p T_0$.

3.4. Triggering methods

Two external ways of the triggering of the negative corona were used: the flux of positive ions and the ultraviolet (UV) radiation.

Flux of positive ions was created by an additional source of positive corona (Figure 7). Two different forms of additional corona were used. When the point electrode of the additional corona source was hemispherically capped, the

26

additional corona existed in the form of positive (steady) glow. In the case of a conical point, there was a pulsed (streamer) corona. The repetition rate of streamers ($\geq 5 \cdot 10^3$ s^{-1}) was determined by the outer circuit of the additional corona.

The flux of ions entering the main discharge gap was changed by changing the rate of the airflow, by the voltage applied to the source of additional corona and by changing the grids G. Grids of mesh size 8, 4, 2, 1.3 and 0.8 mm were used. To diminish a possible influence of the light emitted by the additional corona to the discharge in the main gap, there were small light-tight screens in the central parts of the grids.

The mean current of ions in the main gap was calibrated as a function of the current of the additional corona, the mesh size of the grids and the airflow rate. The calibration was carried out at voltage $\approx$ 500 V below the onset potential of Trichel pulses. In the case of the pulsed form of the additional corona, the amplitude value of the current corresponding to the bunch of the ions was at least three orders of magnitude higher than the mean current.

Our first attempt of UV triggering is described in [66]. For triggering we used the radiation of the laser-formed plasma. XeCl laser created at Pb target, situated behind the plane electrode, a plasma plume. The plume radiated a light pulse of the quasicontinuous spectrum in the range of 200–600 nm. An adequate triggering of Trichel pulses was achieved. Unfortunately, the delay time between the initiating pulse and Trichel pulse changed with time. This effect was related with the dust produced by laser plume: Auger spectrometer detected specks of Pb at the point surface. This drawback forced to find other ways of UV triggering. The final setup of UV triggering is presented in Figure 7.

The deuterium lamp DL (L 6302, Hamamatsu) was used as a source of UV radiation. Quartz lenses L1, L2 directed the radiation to the point surface. By calibrated diaphragms D it was possible to change UV intensity at the point surface by two orders of magnitude.

Using different sets of absorption filters it was estimated that the triggering becomes efficient at wavelength < 350 nm. According to the datasheet of the deuterium lamp [67] and the parameters of the optical system we estimated the number of photons incident on the point surface. It was found that at the wavelength region < 350 nm the photon flux 10^{10} s^{-1} corresponds to the maximum intensity value used. It is a rough estimation and the actual flux of photons may differ from the number presented by an order of magnitude.

The chopper Ch formed rectangular light pulses of 50 µs rise/fall time and usually the duration of pulses was $\approx$ 3.4 ms. The repetition rate of pulses was 50 s^{-1}.

3.5. Recorded discharge parameters

Discharge characteristics change in wide limits. Temporal changes may be as short as a few nanoseconds, which is typical to the rise of Trichel pulses, or as long as 1 h, which is typical for the establishment of the stable emissivity under the influence of UV radiation. Similarly, the order of the smallest detectable current was ≈ 0.1 nA, while the peak of the current of Trichel pulse exceeds 10 mA. For this reason a number of recording devices was used to record the discharge parameters. Table 2 presents the list of the devices used for the detection of the discharge current. The second column presents the lower limits of the current starting from which it was possible to record signals with the given bandwidth and/or rise-time. Where it was possible, the rise-time of the recording system was determined experimentally, using test pulses.

A special attention was paid to suppress the influence of the external electro-magnetic interference. The discharge chamber was screened according to recommendations given in [68] and thus the dominant noise was mainly caused by preamplifiers. In the case of the temporal measurements it was possible for pulses of a good reproducibility (like steady component of LCM) to use the average mode of the digital oscilloscopes, which considerably improved the signal/noise ratio.

Table 2

Phenomenon studied	Range of measured parameters Bandwidth/rise time of the recording system	Equipment
Repetition rate of Trichel pulses		counter C3-34A (Russia)
Waveform of Trichel pulses	> 40 μA 0...500 MHz, $\tau \approx 1$ ns	digital osc Tektronix TDS-540B (sample mode)
Current spikes	> 1 μA 0...100 MHz	preamp (op. amp. NE5539N (Philips)) + digital osc Tektronix TDS-220 (sample mode)
	>1 nA 0...1 MHz	preamp (op. amp. LM318) + digital osc Tektronix TDS-220 (sample mode)
Current of LCM initiated by steady UV radiation	> 0.1 pA	electrometer V7E-42 (Russia)
	> 0.1 nA $\tau \approx 1$s	X-Y recorder EZ-11 (Czechoslovakia)
Current of LCM initiated by pulsed UV radiation	> 1 nA 0...1 MHz, $\tau \approx 5$ μs	preamp (op. amp. LM318) + digital osc Tektronix TDS-220 (average mode)
	> 0.1 nA 0...0.01 MHz	preamplifier (different types) + digital osc Tektronix TDS-220 (average mode)

4. CALCULATION OF BASIC CHARACTERISTICS

4.1. Field distribution

As we found, [69], for calculation of the discharge parameters in electronegative gases the use of different approximation formulae for field distribution does not give satisfactory coincidence with the experimental results. For this reason we modelled the field distribution for the point-plane gap used. In the calculations the influence of the discharge chamber walls on the field distribution was also taken into account.

The distribution of the Laplacian electric field $E(x,r)$, where r denotes the distance from the gap axis, was calculated numerically. The rectangular computation domain was first divided into a uniform square grid having 5 nodes per millimetre. The domain was set a little larger than the discharge gap. On the gap axis, the condition of symmetry was used. In the vicinity of the point electrode (about 1 mm around the point electrode tip), we made additional iterations. The domain was divided into a square grid having 100 nodes per millimetre.

The potential of each node was calculated using finite difference method together with the successive over-relaxation method [70]. For the convergence criterion of the iterations there was the requirement that the relative residual in the iterative process should not exceed 10^{-14} at each interior node.

The accuracy of the computing algorithm was tested by the numerical evaluation of the well-known field distributions of coaxial cylinders and concentric spheres. The difference between analytical and numerical results was less than 0.5%.

Finally, the electric field strength was found for each node using the values of potential of that node and surrounding nodes.

To check the calculation quality of the electric field strength, we have calculated the normalization integral. It differs from the applied voltages less than 10 V.

Figure 9 gives the distribution of the equipotential lines. The distributions of equipotential lines for stressed plane and point differ considerably. In the case of the stressed plate in the remarkable part of the space between the electrodes, the field is almost homogeneous both in axial and radial directions.

Figure 10 gives field distributions calculated at voltages corresponding to the inception voltages of Trichel pulse of a certain point electrode. As it should be, in the ionisation zone the field distributions coincide with each other (Figure 10A). In the drift zone, the axial components of the fields have a big difference (Figure 10B): in the case of the stressed plane electrode, the field is much higher than it is for stressed point electrode.

29
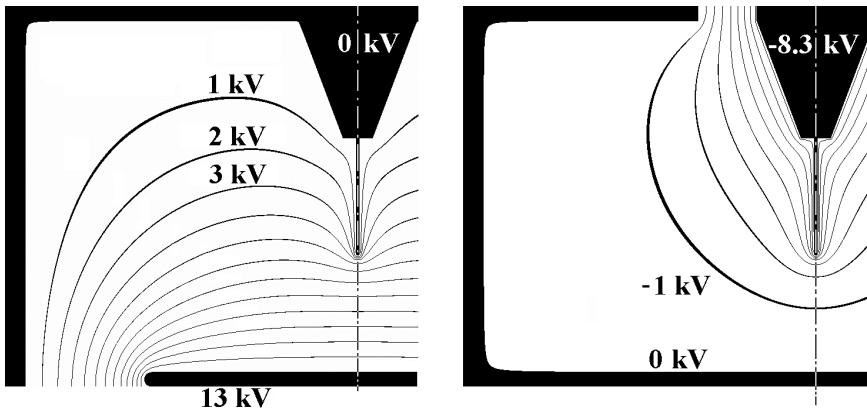
Figure 9. Equipotential lines in the case of stressed anode (left) and stressed cathode (right).
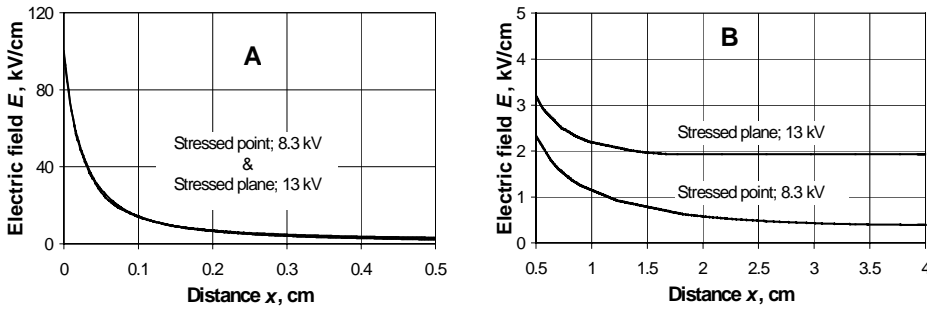
Figure 10. Field distribution along the gap axis at the onset of Trichel pulses; A — ionisation zone; B — drift zone.

4.2. Drift time and ionisation integral

For drift velocities of electrons, v_e, and positive ions, v_p, as well as for ionisation coefficient α and attachment coefficient η we used the formulae given in [71]. The formulae based on the experimental data of [72]. In the case of negative ions one should consider besides the electron attachment also the detachment and conversion processes [73, 74]. According to our test calculations, the influence of the detachment was negligible because of the very limited extent of the high field region, and the conversion was practically a simultaneous process.

30

For these reasons both the ionisation and attachment were characterised by one coefficient, α_{eff} .

For the mobility of negative ions μ_n (cm^{2}V^{-1}s^{-1}) we used the experimental data from [72], the best fit of the data was

$$\mu_n = 2.31 - 0.0056(E/p) \qquad E/p > 19.64 \text{ V·cm}^{-1}\text{·Torr}^{-1}$$
$$\mu_n = 2.2 \qquad\qquad\qquad \text{otherwise.}$$

It should be mentioned that the calculated value of O_2^- mobility at low values of the electric field strength is 3.3 cm^{2}V^{-1}s^{-1} [75]. The discrepancy between the measured and calculated values of the mobility could be explained by the conversion of the simple ions into complex ones. In air and for times $> 10^{-7}$ s $O_2^-(H_2O)_n$ ions are the dominating ones [76]. The mobility values used in our calculations correspond to $n = 4$–5 of $O_2^-(H_2O)_n$ ion.

The electrical wind may influence the movement of the negative ions in the drift zone [77]. In our case the effect was very small compared with the drift velocity in the electric field.
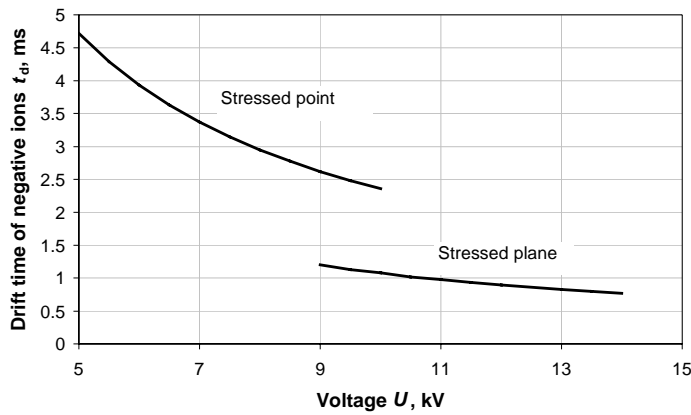
**Figure 11.** Drift time t_d of negative ions from point to plane as a function of voltage.

Figure 11 demonstrates that the remarkable difference of the field distributions for stressed point and plane in the drift zone causes more than two times difference of the drift times of negative ions. Figure 12 gives the time $\Delta t_d = \int_0^x dx / v_n$ as a function of the distance from the point electrode.

31
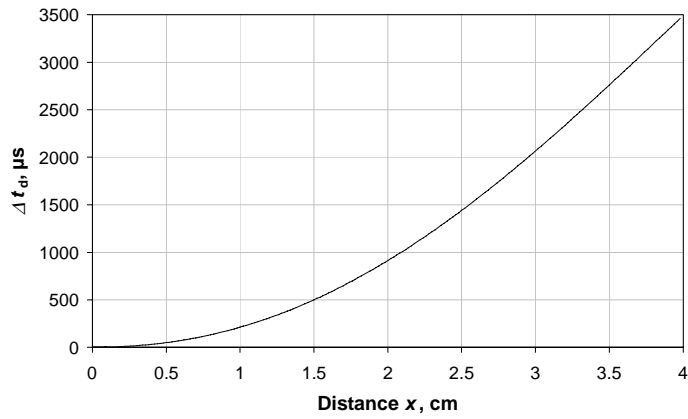
Figure 12. Drift time of negative ions, Δt_d, versus distance from the point; stressed point, $U = 8.2$ kV.

According to Figure 13 the numbers of electrons in an avalanche, $\exp(\int \alpha_{eff}\,dx)$, calculated at the onset of Trichel pulses for stressed point and stressed plane, are very close. Once again, the result confirms that the onset phenomena are mainly determined by the field distribution in the ionisation zone.
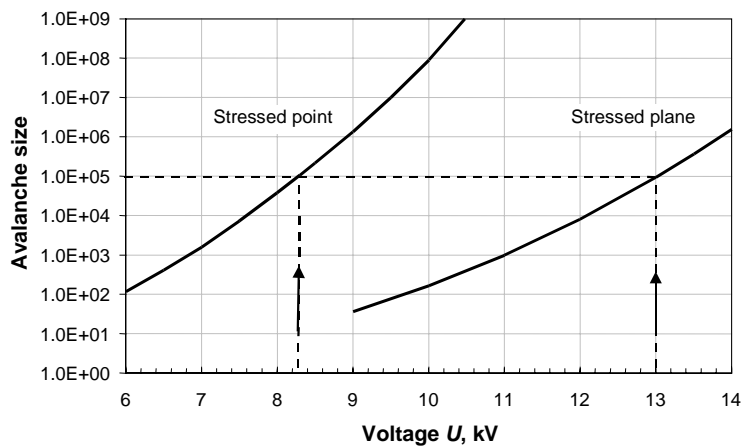
Figure 13. Number of electrons in an avalanche as a function of voltage; arrows indicate the avalanche sizes at the onset potential of Trichel pulse.

As calculations showed, for used discharge gap geometry the values of $\exp(\int \alpha_{eff}\,dx)$ and $\exp(\int \alpha dx)$ are very close. It means that the number of positive ions created by an avalanche equals to the number of electrons. The reason

32

of this coincidence is that in our case the attachment occurs at the distances from the point where the ionization is practically missing.

4.3. Current components of avalanche

The current in the external circuit of the discharge gap was calculated according to Ramo - Shockley theorem [78, 79].

To calculate the electron component of the avalanche current, the gap was divided into discs, the thickness Δx of which in the axial direction was 1 μm. It was assumed that at any time instant the electrons are only in one disc, i.e. we neglected the diffusion. The amount of electrons in a disc k was calculated as $N_e(k) = [\alpha_{eff}(k)\Delta x + 1]N_e(k-1)$, and the current of the electron component as

$$i_e(t_k) = e\frac{E_k}{U}N_e(k)\mathrm{v}_{ek} \text{ where } t_k = \sum_k \frac{k\Delta x}{\mathrm{v}_e(k)}.$$

It was assumed that during the drift of the electrons the ions do not move. The number of positive and negative ions in the disc k is $N_p(k) = \alpha(k)N_e(k-1)\Delta x$ and $N_n(k) = \eta(k)N_e(k-1)\Delta x$, respectively. To calculate the current of positive ions the gap was split into discs with thickness, Δx_p, which corresponded to the distance that ions pass during 10 ns, i.e. the thickness of the discs changed in the space. In the case of negative ions for times $t < 190\mu s$ the thickness of a disc, Δx_n, corresponded to the time interval $0.1\mu s$, and if $t \geq 190\mu s$, $1\mu s$ step was used. Then we found the amount of ions in discs Δx_p and Δx_n and calculated the current. To calculate the current at the next time moment the ions were lifted to the next disc.

As it was tested, the results received by this procedure did not differ remarkably from those received using more sophisticated (and considerably more time-consuming) algorithms.

As it follows from Figure 14, the peak value and duration of current components have a huge difference.
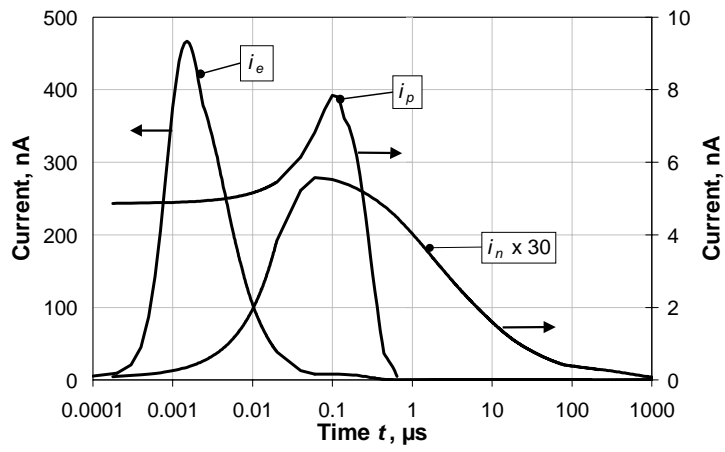
Figure 14. Calculated waveforms of current components; i_e, i_p, i_n — electron, positive ion and negative ion components, respectively; stressed plane, $U = 13$ kV.

5. TRIGGERED TRICHEL PULSES

This chapter presents results concerning the studies of the repetition rate of Trichel pulses.

5.1. Common regularities

For a certain point type only the applied voltage was not the only factor determining the repetition rate of Trichel pulses. For all points tested we observed long-term memory effects e.g. the repetition rate depended on how long was the break between two measurement cycles. Memory effects were recorded even when the morphological changes of the point surface were not detectable. When the break was comparatively short (<1 h) the first spontaneous (i.e. externally non-triggered) Trichel pulses started in the stagnant air at the voltage range $U_0 = 8.1–8.3$ kV. Near these onset potentials the train of Trichel pulses was very irregular.

We found, [80], that the repetition rate of Trichel pulses in airflow was always smaller than in stagnant air. When the break between two measurement cycles was half an hour or more, the spontaneous Trichel pulses did not appear even at voltages exceeding considerably the onset potential U_0 (Figure 15). UV radiation of low intensity triggers pulses starting from a voltage which is close to the onset potential U_0. Ions are able to trigger discharge at voltages $U < U_0$ but in this case the repetition rate increased with the voltage more slowly. When for triggering UV radiation and ion flux were used simultaneously, the rate of the growth of the repetition rate is close to that of UV triggering and further lowering of the inception voltage of Trichel pulses is recorded. Using external means of triggering, very regular trains of Trichel pulses were achieved: each point in Figure 15 presents the average value of 12 recordings. Even at the lowest repetition rates the standard deviation was less than 20%.

Figure 16 presents the relationship between the repetition rate and the mean current of corona. The dependencies for both triggering methods are linear but the slopes are slightly different. As the slope gives the charge per Trichel pulse, q_{Tr}, it seems that ion-created Trichel pulse is somewhat larger. The average value of the charge per pulse was $q_{Tr} \approx 7 \times 10^{-10}$ C.
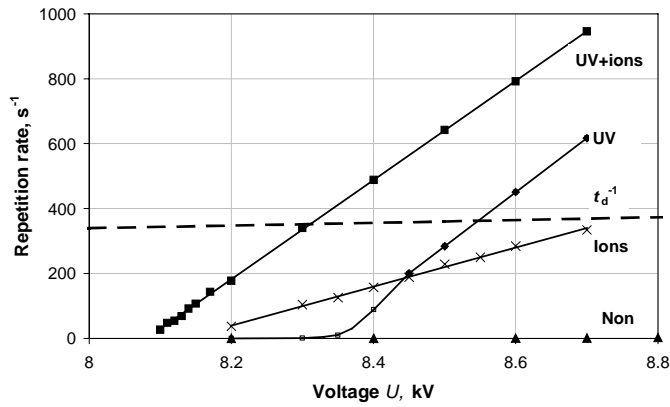
Figure 15. Repetition rate as a function of voltage; labels indicate the manner of triggering; dashed line — reciprocal of the drift time, t_d, of the negative ions in the gap; stressed point.
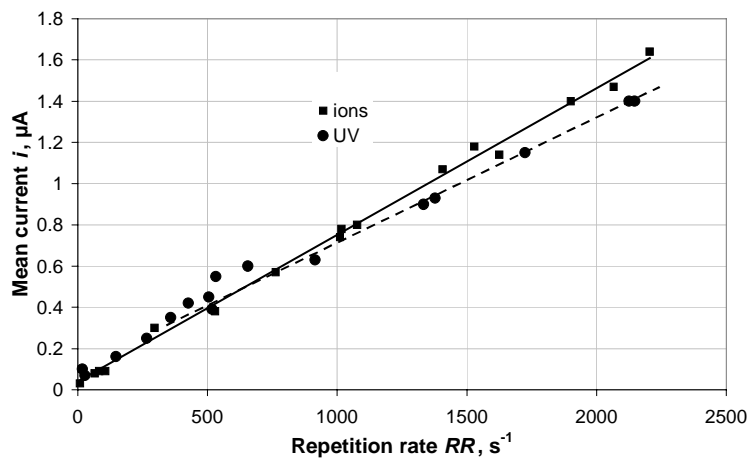

Figure 16. Mean current versus repetition rate; Pt point; Trichel pulses are triggered by positive ions and UV radiation.

5.2. Triggering by flux of ions

All the figures presented in this section belong to the initiation by the steady flux of ions. In the case of triggering by pulsed ion flux the regularities were the same but the standard deviation of the repetition rate was larger. The values of the ion current presented were recorded at the voltage 6.9 kV. A good repro-ducibility of the results was achieved when the time interval between the settings of the new values of the voltage, U, and the ion current, i_i, was at least 10 min.

As it follows from Figure 17, at a fixed value of the ion current the repetition rate is a linear function of the voltage; the slope of the dependence increases with the ion current. Besides, there is a certain minimum value of the ion current starting from which the triggering becomes efficient. The growth of the ion current reduces the inception voltage of Trichel pulses. Figure 18 presents the decrease of the inception voltage, $\Delta U = U_{min} - U_{thr}$, as a function of the ion current. Here U_{min} corresponds to the minimum value of the ion current starting from which the triggering becomes possible. Every point type had its own characteristic value of the ion current starting from which Trichel pulses were triggered (Figure 19).
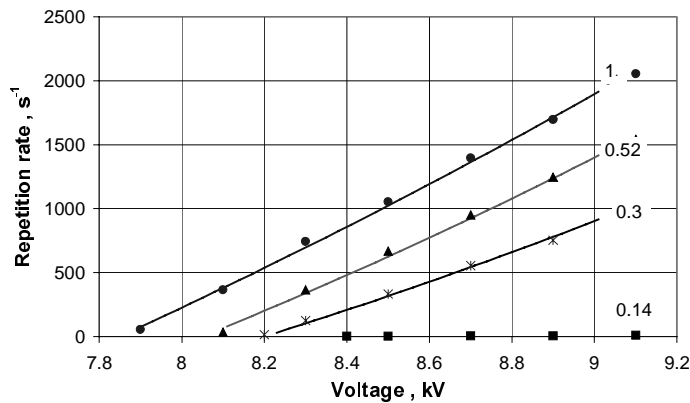
Figure 17. Repetition rate as a function of voltage; labels — current of ions, μA; Cu + 70 nm TiO$_2$ point; stressed point.

37
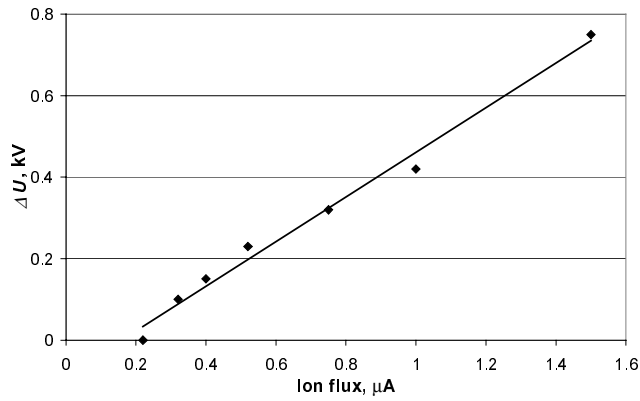
Figure 18. Decrease of the threshold voltage as a function of the ion current; Cu + 70 nm TiO_2 point.
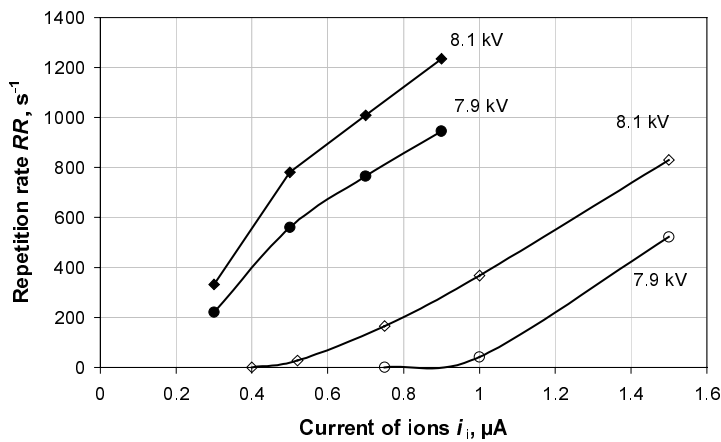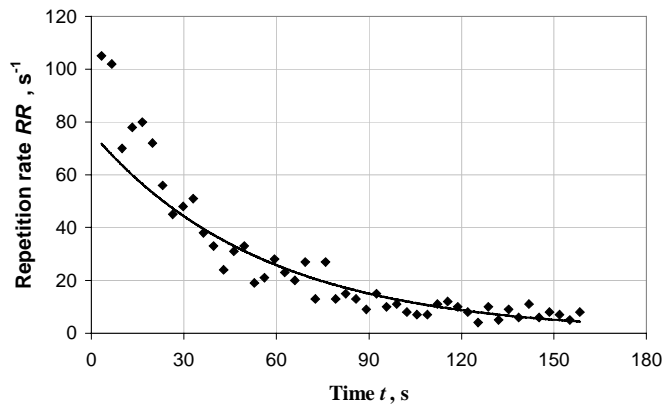

Figure 19. Repetition rate as a function of voltage; labels — applied voltage; filled symbols — Pt point; open symbols — Cu + 70 nm TiO_2 point; stressed point.

A set of the dependencies in Figure 20 is typical for all the point types studied: initial fast rise of the repetition rate with the ion current is replaced by slower linear growth at higher ion currents. At the linear parts of the curves the slope for all voltages is almost the same. It is remarkable that the dependencies become linear nearly at the same value of the ion current.
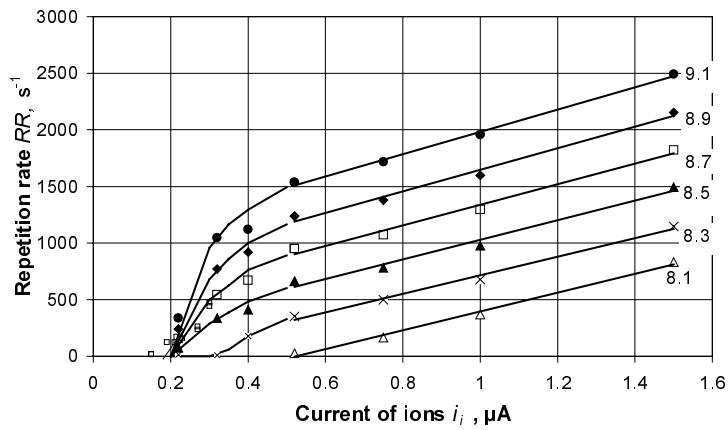
Figure 20. Repetition rate as a function of ion current; labels — applied voltage, kV; Cu + 70 nm TiO_2 point; stressed point.

Figure 21 presents the diminishing of the repetition rate after the interruption of the ion flux.
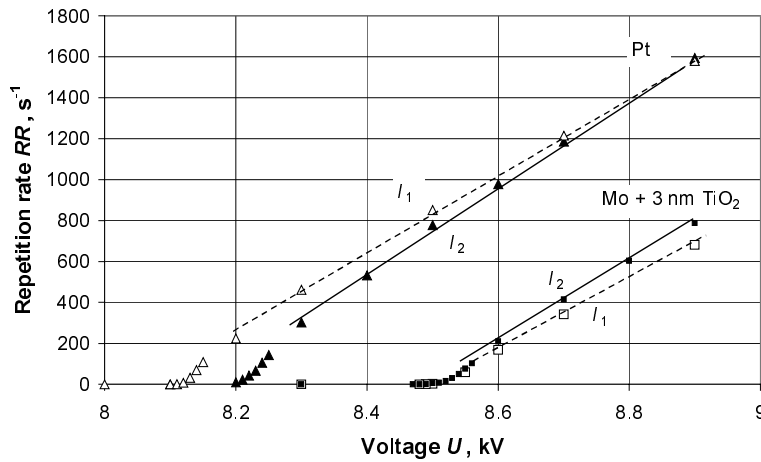

Figure 21. Repetition rate as a function of time; at the moment $t = 0$ the flux of ions was interrupted; non-oxidised Cu point; stressed point, $U = 8.1$ kV; solid line corresponds to the exponential decay of ≈ 16 s time constant.

39

5.3. Triggering by steady UV light

Like in the case of the ion triggering the measurements were carried out in airflow. Before the recording of the repetition rate the point electrodes passed a conditioning procedure: they were exposed to UV radiation at voltages below the inception voltage of Trichel pulses. After this procedure a very good reproducibility of the dependencies was achieved even at low values ($< 100 \text{ s}^{-1}$) of the repetition rate.

The inception voltage of the triggered pulses depends both on the point type and UV intensity. In contrast with the ion triggering the inception voltage was never lower than the onset potential, U_0, of the spontaneous Trichel pulses in the stagnant medium. The difference between the inception voltages for different point types was large (Figure 22). As a rule, higher intensities of UV radiation shifted the inception voltage towards its higher values. The effect was especially pronounced for Pt point. Apart from the voltages very close to the inception voltage, the repetition rate was a linear function of voltage. At a fixed voltage the repetition rates for various point types differ considerably but the slopes of the dependencies are close.
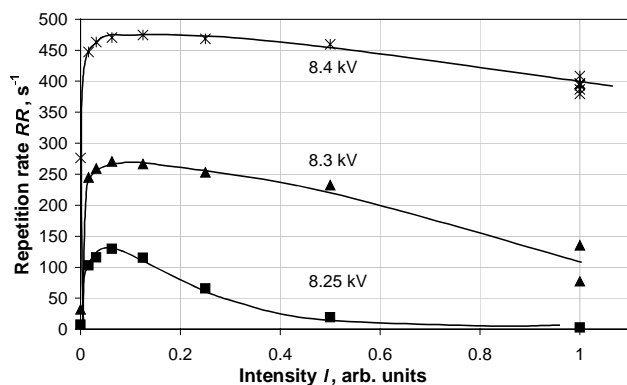

Figure 22. Repetition rate as a function of voltage for different point types; two intensities of UV radiation, $I_2 \approx 4I_1$; stressed point.

In contrast with the ion triggering, for UV triggering the threshold value of the intensity was missing: Trichel pulses were triggered even by UV radiation scattered from the walls of the discharge chamber. Figure 23 demonstrates that near the inception voltage the growth of UV intensity causes the saturation of the repetition rate. The saturated values of the repetition rate have a very strong

dependence on voltage. Furthermore, for Pt point UV radiation may totally suppress Trichel pulses (Figure 24).
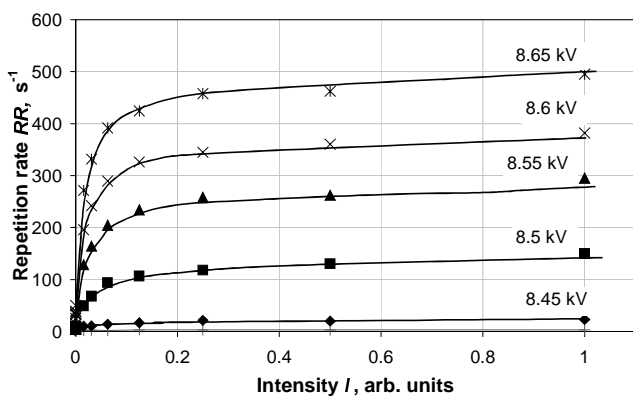
Figure 23. Repetition rate as a function of UV intensity for different voltages; Mo + 1 nm TiO_2 point; stressed point.

Figure 24. Repetition rate as a function of UV intensity for different voltages; Pt point; stressed point.

5.4. Influence of space charge

As it is widely accepted [9, 11], and proved by modelling [12], the repetition rate of Trichel pulses is controlled by the space charge of negative ions. At the same time the above-presented dependencies indicate that the repetition rate is also influenced by the point type and the intensity of the triggering source.

In order to check the influence of the negative ions accumulated in the gap, the space charge field was calculated using the method of discs [81]. In calculations the effect of mirror charges was taken into account. It was set that the charge of negative ions equals to the charge produced by a Trichel pulse. In our calculations we neglected the longitudinal diffusion, i.e. it was supposed that during the drift the negative ions of a Trichel pulse are concentrated in the limits of one disc. Like in [12] we supposed that the cloud of negative ions drifting towards the anode widens in the direction perpendicular to the gap axis, according to the Warburg law [82], but in calculations we used the values of the field strength at the gap axis.

The calculations were carried out for stressed point at voltage $U = 8.2$ kV. The positions of space charge clouds belonging to subsequent Trichel pulse, were determined on the basis of Figure 15. Figure 25A presents the field distribution caused by negative ions for a hypothetical case when the repetition rate is 5000 s^{-1}. Compared with Laplacian field (Figure 10) the distortion of the electric field distribution in the ionisation zone is considerable. Similar calculations made for repetition rate 1000 s^{-1} showed that the total reduced field at the point surface diminishes only by 0.4 $Vcm^{-1}Torr^{-1}$.

As it follows from Figure 25B even at repetition rate 1000 s^{-1} the space charge causes remarkable reduction of the avalanche size. As the drift time of negative ions moving out of the gap axis is longer, the influence of the space charge should appear even at lower repetition rates.

Figure 26 is a good demonstration of the effect of the negative space charge. Here the discharge is triggered by UV pulse of 4 ms duration (more details of the discharge triggered by the pulsed UV light are presented in the section 6.3). The peaks of Trichel pulses are cut off and the long low-current tails of pulses correspond to the drift of negative ions. The mean time interval between Trichel pulses presented in the figure, is 0.95 ms which corresponds to the repetition rate ≈ 1000 s^{-1}.

The latter value of the repetition rate belongs to the stressed plane. According to Figure 11 near the onset of Trichel pulses the drift time of negative ions for stressed point exceeds that for stressed plane more than three times. Therefore already at repetition rates > 300 s^{-1} the accumulation of the negative space charge could influence the discharge parameters.
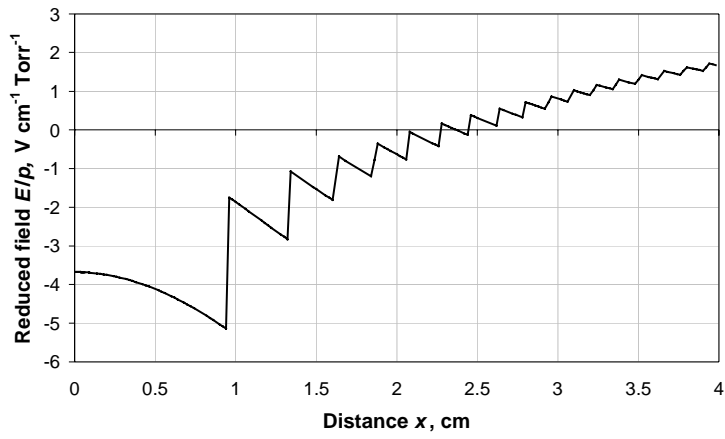
Figure 25A. Field distribution caused by the space charge of negative ions; $U = 8.2$ kV; stressed point; repetition rate — 5000 s^{-1}.
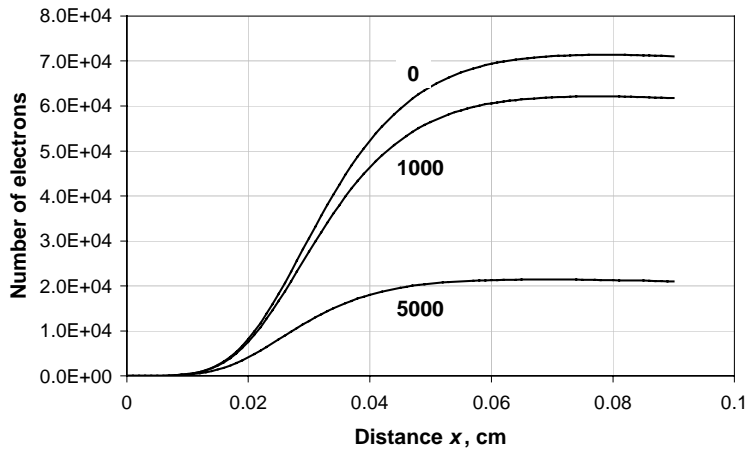
Figure 25B. Growth of avalanches in space; labels correspond to different repetition rates; $U = 8.2$ kV; stressed point.

43
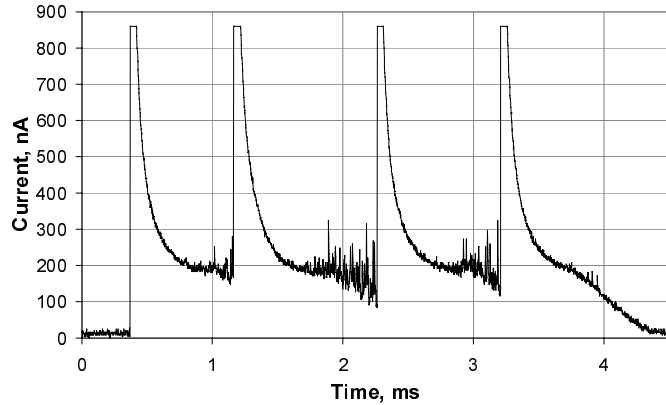
Figure 26. Trichel pulses triggered by 4 ms UV pulse; Pt point; UV intensity $I = 0.016\, I_0$; $U = 12.6$ kV, stressed plane.

The space charge effect explains easily the large difference between the repetition rates recorded at a fixed voltage for two point types (Figure 22). Indeed, let's assume that the coefficient of the secondary emission, γ, is larger for Pt point. Thus, if the equality $\gamma \exp\left(\int \alpha_{eff}\, dx\right) = 1$ is the condition of the rise of Trichel pulse, the pulse arises at lower fields. Consequently, for this point the space charge has a smaller influence i.e. the repetition rate achieved at a fixed voltage is higher.

Nevertheless, some results indicate that the space charge is not the only factor determining the repetition rate. For instance the repetition rate increases with the voltage faster than it follows from the decrease of the drift time of negative ions. Indeed, increasing the voltage from 8 to 9 kV diminishes the drift time from 3 to 2.4 ms (Figure 11). At the same time the repetition rate increases more than four times (Figure 20). Even more drastic growth follows from Figure 23: the growth of the voltage by 0.2 kV leads to the increase of the repetition rate by ten times.

6. LOW CURRENT MODE

The chapter deals with the experimental study of processes leading to the rise of Trichel pulses.

6.1. Conditioning

As it was described in previous chapters, such important characteristics of Trichel pulses like the inception voltage and the repetition rate have a strong dependence on the prehistory of the point electrode. For this reason many reports in the field of negative corona contain a remark like 'before the recording of the discharge parameters the point electrode was conditioned'. The conditioning guarantees a satisfactory reproducibility of the recordings but as a rule the actual meaning of the conditioning remains unopened. It appeared that in the case of the low current mode of the discharge the memory effects play even more crucial role. Therefore we tested the long-term changes of the discharge as a function of influencing factors.

The recordings were carried out at voltages where UV radiation was not able to trigger Trichel pulses. When the point was not illuminated the current was less than 10^{-12} A. The latter value corresponded to the noise level of the recording system.

At set values of the voltage and UV intensity the current depended on the rate of the airflow. Before the switch-on of the airflow the gap was stressed and the point was illuminated during half an hour. Figure 27 reflects a typical long-term change in the discharge current after the switch-on of the airflow at $t = 0$. This effect was reversible i.e. if the airflow was switched off, the current decay was observed during the same characteristic time interval. The current value established after the conditioning period became independent on airflow rate if the latter exceeded 3.5 ms^{-1}. The time interval needed for conditioning was different for different point types.

Another medium parameter influencing the current of LCM was temperature. At fixed values of the voltage, airflow rate and UV intensity a small growth of the temperature caused the current increase by nearly 50% (Figure 28). As the change of the reduced field due to the diminishing of the gas density was negligible, the effect might be related only with the emissivity of the point electrode.
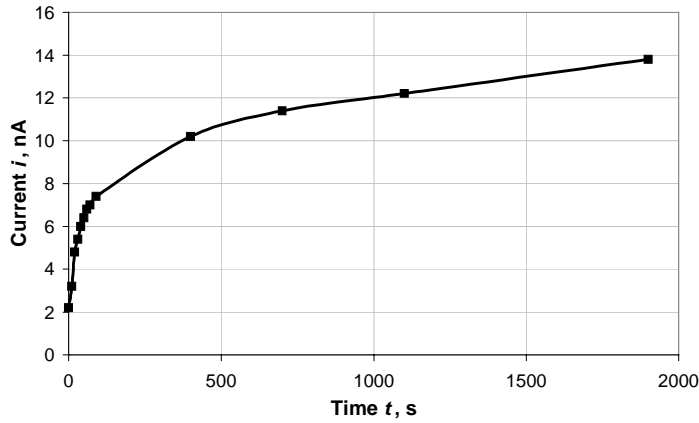
Figure 27. The influence of airflow on discharge current; airflow was switched on at $t = 0$; Pt point; $U = 7.4$ kV; stressed point.
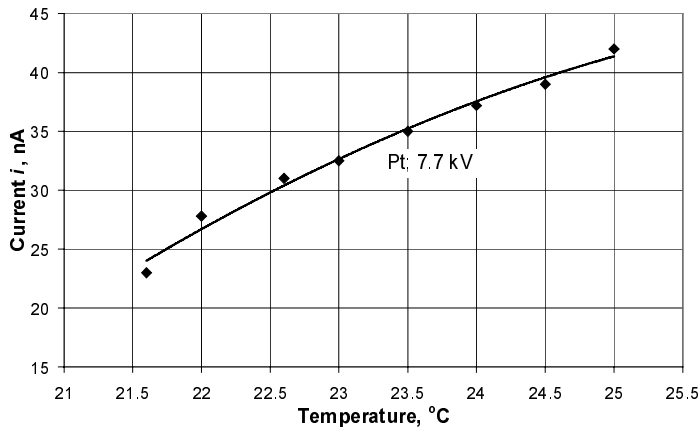

Figure 28. Current as a function of temperature; airflow rate — 4.4 ms^{-1}; stressed point.

At a fixed voltage after the switch-on of UV radiation the stationary value of the current establishes during a final time interval. This interval depended on point type (Figure 29) and it was the largest for Pt point.

46
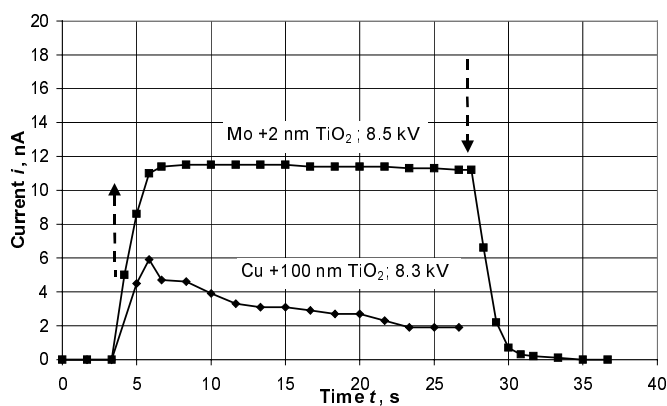
Figure 29. Temporal changes of the photoinduced current; arrows indicate the moments when UV radiation was switched on/off; airflow rate — 4.4 ms^{-1}; stressed point.

Furthermore, the rise-time of the current depended on how long was the break between two successive measurements (Figure 30). In the case of 16 h break the discharge gap was not stressed, but during 15 min break only UV radiation was missing.
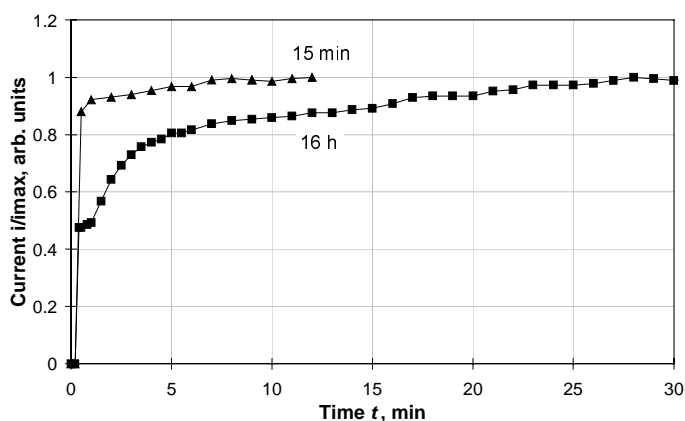
Figure 30. Current as a function of time; labels indicate the duration of the break of UV illumination; Pt point; airflow rate — 5.3 ms^{-1}; $U = 8.4$ kV, stressed point.

A point once conditioned maintains its emissivity during a long time interval. Before recording the dependence in Figure 31 the point was conditioned at voltage 8 kV and at maximum UV intensity, $I = 1$, the corresponding current

47

value was 150 nA. At the moment $t = 0$ the voltage was switched to 6.8 kV. To establish a new stationary value more than three hours were needed and the process was influenced only a little by interim minute-range changes of UV intensity.
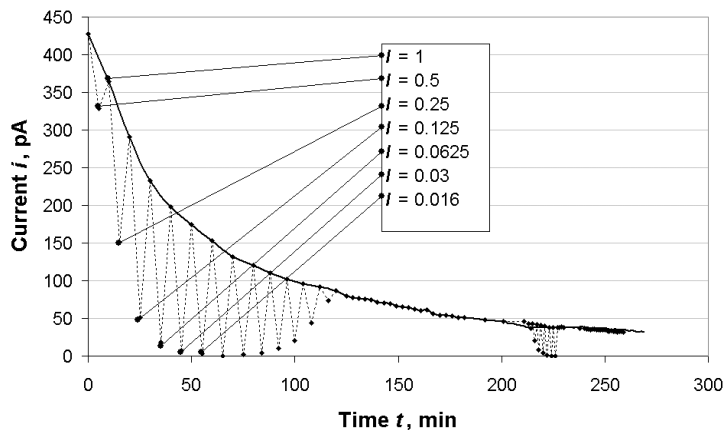
Figure 31. Current as a function of time; Pt point; $U = 6.8$ kV, stressed point; airflow rate — 3.5 ms^{-1}; I — UV intensity, arb. units; solid curve follows the dependence for maximum UV intensity.

As it was explained above, there are many factors that influence the current of LCM. Negligence of these regularities impedes the achievement of reliable results. For this reason all points tested passed the following procedure. Before the measurements the airflow was switched on and a point was exposed to UV light of maximum intensity. During the exposition the applied voltage was ≈ 100 V below the inception voltage of Trichel pulses. The duration of the conditioning time was half of hour. The procedure guaranteed a good day-to-day reproducibility of the results.

6.2. Current induced by steady UV light

Under our experimental conditions i.e. in a dust free airflow LCM is non-self-sustained. This section includes the results dealing with the current of LCM induced by the steady UV radiation. The upper limit where the current was recorded coincided with the inception voltage of Trichel pulses. First the results of our studies in this field were published in [7 (**Paper I**)].

As it follows from Figure 32 even in air at atmospheric pressure the cathodes without special coatings have considerably different quantum yields of photo-emission (emitted electrons per incident photon). But a more important finding

48

is that the relationship between the quantum yield and the substrate material is missing. Indeed, the workfunctions of Pt and Mo are 5.65 and 4.6 eV, respectively, while the quantum yield of Pt point exceeds that of Mo by more than three orders of magnitude.
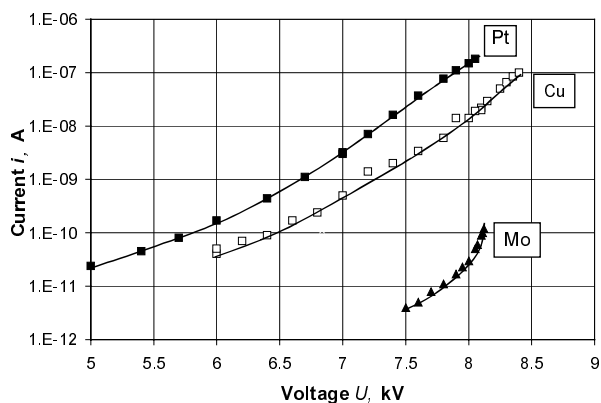
Figure 32. Photoinduced current as a function of voltage recorded at a low value of UV intensity; stressed point.

Artificial coatings change substantially the emissivity of the electrode (Figure 33). The discharge current depended not only on the coating material but also on its thickness. From the viewpoint of the enlargement of the quantum yield thin layers are the most efficient. At the same time the inception voltages of Trichel pulses recorded at low UV intensities seemed to remain unchanged.
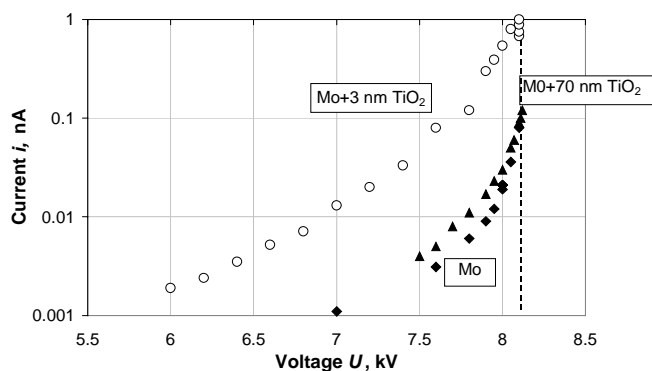

Figure 33. Effect of the electrode coating on the current; dashed line indicates to the inception voltage of Trichel pulses; stressed point.

49

At a fixed voltage and for all point types the photoinduced current was a non-linear function of UV intensity. The same trend of the saturation was recorded independently on how large was the current corresponding to the maximum UV intensity. Figure 34 gives a typical current-versus-intensity dependence. The currents, i_{max}, corresponding to the maximum UV intensity, were recorded at voltages 8.06 kV (Mo + TiO$_2$ point) and 7.93 kV (Cu + HfO$_2$ point). The similar behaviour was characteristic for points where the maximum current was of 1 μ A range (Pt and Cu + CuI points).

For point types of a comparatively large value of the quantum yield it appeared that larger values of UV intensity shift the inception voltage of Trichel pulses towards higher values of the voltage. Recording of the dependencies in Figure 35 was stopped when Trichel pulses appeared.
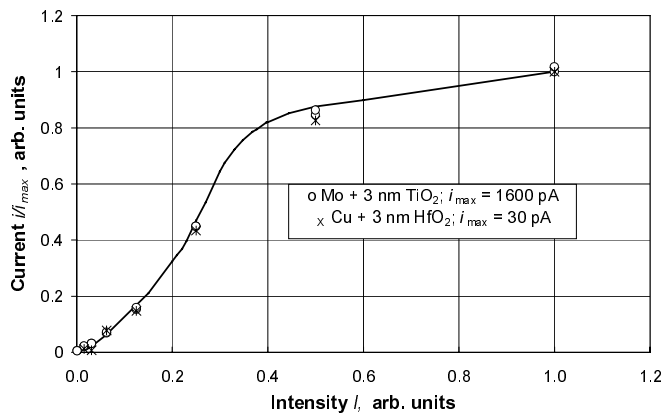
Figure 34. Current as a function of UV intensity; stressed point, corresponding voltages are in the text.
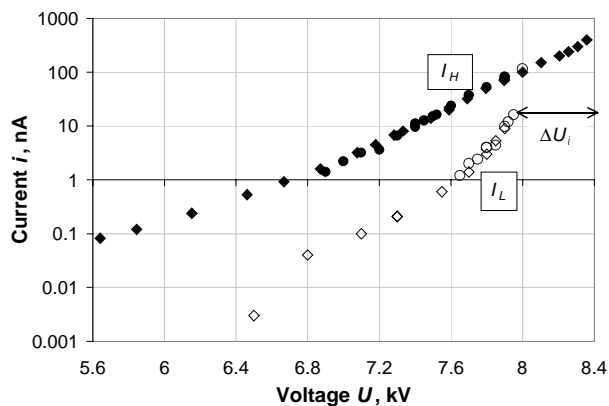
Figure 35. Current as a function of voltage for two UV intensities; $I_H \approx 10\,I_L$; ΔU_i — the shift of inception voltage; Pt point, stressed point.

50

6.3. Current induced by pulsed UV light

In the section 6.2 we described a non-linear dependence of the photoinduced current on UV intensity. Although it seems that the trend of saturation was not related with the current value, still the space charge of negative ions could have some influence on the discharge characteristics. For this reason in the next cycle of the experiment UV pulses of a low repetition rate triggered LCM of the discharge. In this case the space charge of negative ions produced during the previous pulse does not influence the discharge during the next UV pulse. Before the measurements the points passed the same conditioning procedure like described previously.

In [83] we found that during the rise of UV pulse the current growth does not follow that of UV intensity and the current increase seemed to depend on the point type.

6.3.1. Common regularities

Further all UV intensities are related with I_0 for which we estimated the value of the photon flux incident on the surface of the point electrode.

In Figure 36 there is a series of the current pulses triggered by UV pulses of 50 s^{-1} repetition rate. During the recording the voltage was set just at the inception voltage, U_i, and so not each UV pulse led to the rise of Trichel pulse. At lower voltages only pulses of LCM were recorded. A more detailed insight of LCM pulses clarified that they have a complicated structure. Besides the steady component of LCM current there were short-duration current spikes that have a peak value which exceeds considerably the current level of the steady component. The voltages where the current spikes were detectable were related to the inception voltage, U_i, of a certain point type and not to the absolute value of the voltage. Because of the limited number of recording points Figure 37 does not pass the actual size of the current spike.
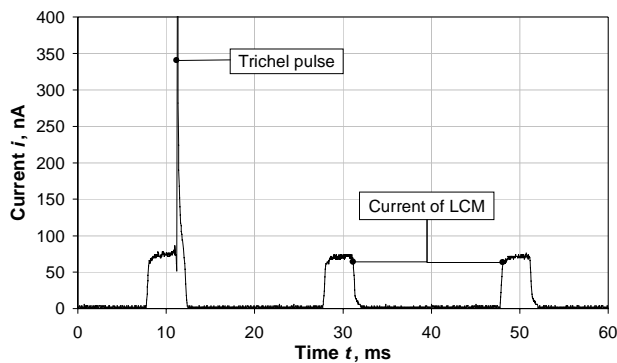

Figure 36. Series of current pulses induced by UV pulses; UV intensity $I = I_0$; Mo + 1 nm TiO$_2$ point; $U = 12.7$ kV, stressed plane.

51
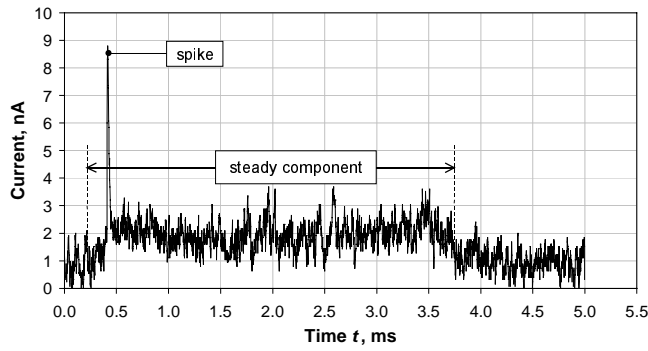
Figure 37. Two components of LCM current; UV intensity $I = 0.016I_0$; Mo + 1 nm TiO_2 point; $U = 12.65$ kV, stressed plane.

At voltages more than 100 V below the inception voltage only the steady component of LCM current was detectable. The waveforms of the steady component recorded in the case of stressed point and plane differ considerably (Figure 38). Compared with the stressed point LCM current of the stressed plane had a shorter duration and after a transition period it reaches a nearly constant value, further named as the plateau current, i_{Pl}.
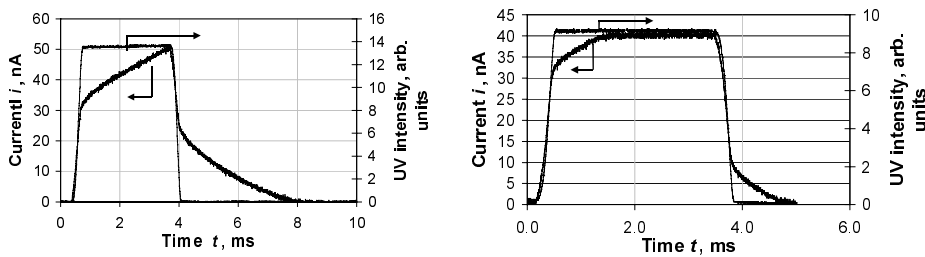
Figure 38. UV pulse and steady component of LCM; left — stressed point; right — stressed plane.

6.3.2. Steady component of LCM

This subsection presents the results of the experiments carried out at voltages where only the steady component of LCM arises. Current waveforms were measured for several point types changing both voltage and UV intensity.

The regularities of the current waveform in Figure 39 were typical for all point types at lower voltages and/or at low values of UV intensity. First, the current rises with a rate comparable with that of the light pulse. The next current

52

increment lasts $t_{dr} \approx 1$ ms and then the current reaches its plateau value, i_{Pl}. At the end of UV pulse the current passes the same fast and slow stages like at the beginning of the pulse. The slow stage of the current decay takes place when the point illumination is already missing.
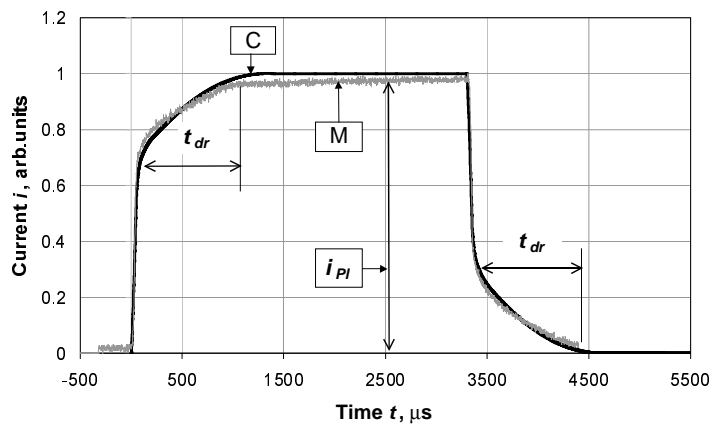
Figure 39. Normalized waveforms of measured (M) and calculated (C) current pulses; stressed plane; other symbols are explained in the text.

For point types (e.g. Pt, Cu, Cu + CuI), having large values of the quantum yield the growth of the voltage and/or UV intensity leads to the appearance of an overshot at the beginning of the current pulse. According to Figure 40 the magnitude of the overshot increases with the growth of UV intensity.
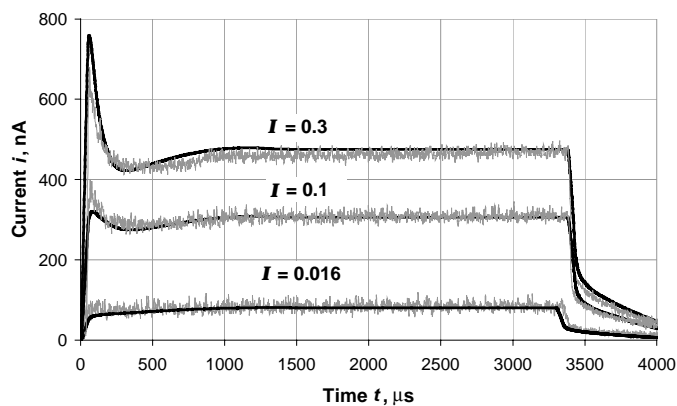
Figure 40. Cu + CuI point; waveforms of the current at different UV intensities I; $U = 13.5$ kV, stressed plane; smooth curves present the results of calculations.

53

The plateau current, i_{Pl}, is a non-linear function of UV intensity (Figure 41). This sub-linear dependence is characteristic even for points of small values of the plateau current [84 (**Paper III),** Figure 4] but compared with the similar dependencies carried out at steady UV radiation (Figure 34) the trend of the saturation is less pronounced. Figure 42 demonstrates that deviation from a linear dependence increases with the voltage growth.
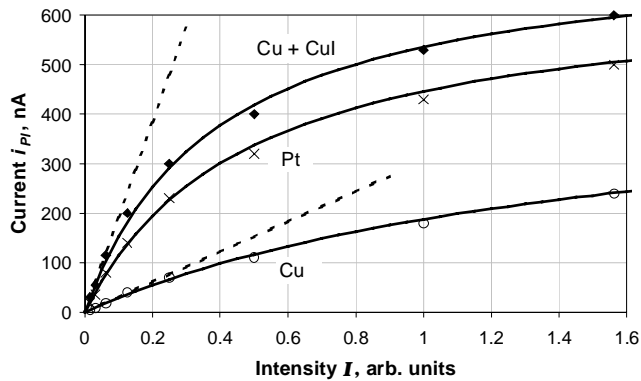
Figure 41. Different types of point electrodes; current i_{Pl} as a function of the intensity I; $U = 12.5$ kV, stressed plane; points are results of experiment; lines are results of calculations.
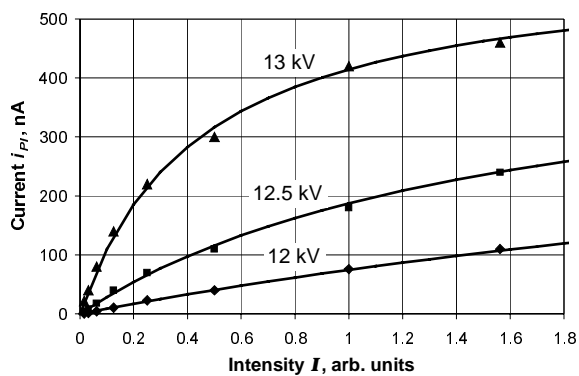
Figure 42. Cu point; plateau current i_{Pl} at different voltages as a function of intensity; stressed plane; points are results of experiment; lines are results of calculations.

6.3.3. Current spikes, transition to Trichel pulse

First we described spikes in [7 (**Paper I**)], the results of more detailed studies are presented in [59 (**Paper II**), 85].

As it was mentioned (subsection 6.3.1), at voltages close to the inception voltage, U_i, current spikes appear besides the steady component. The spike in Figure 43A was recorded at the largest possible bandwidth of the recording system, which still allowed to separate the useful signal from the noise. As it was checked the current oscillations before and after the spike are caused by the noise and not by the fluctuations of the steady current component.

The waveform of the current spike was recurring (Figure 43 A, B) and it did not depend neither on the point type nor on the value of the plateau current of the steady component.
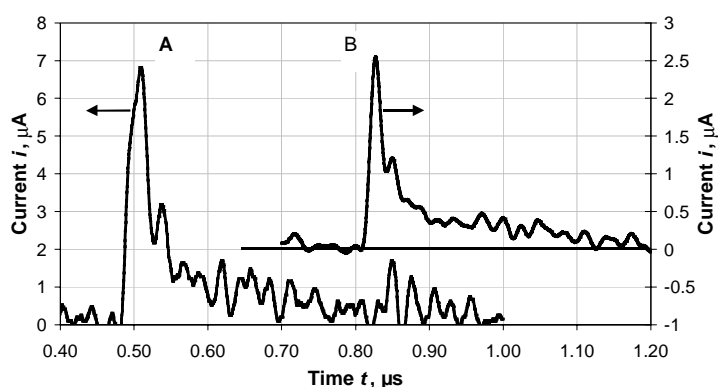
Figure 43. A — single spike; B — average of 16 spikes recorded at the same triggering level of the oscilloscope as the single spike.

During UV pulse several current spikes started but only the characteristics of the very first current spike was studied. The peak of these pulses varied, the smallest detectable spike had the peak value of 1 μ A. Figure 44 gives the amplitude distribution of first spikes recorded at a voltage just below the inception voltage of Trichel pulses. Figure 45 presents the temporal distribution of the first spikes during UV pulse. The moment of the appearance of the first spike depended on the level of the plateau current. The higher was the level the earlier the first spike started. As a rule when $i_{Pl} > 100$ nA, the spike raised at the first front of UV pulse. Besides, the growth of the plateau current lead to the diminishing of the total number of spikes arising during UV pulse. Large values of the plateau current could totally suppress spikes (Figure 46).

55

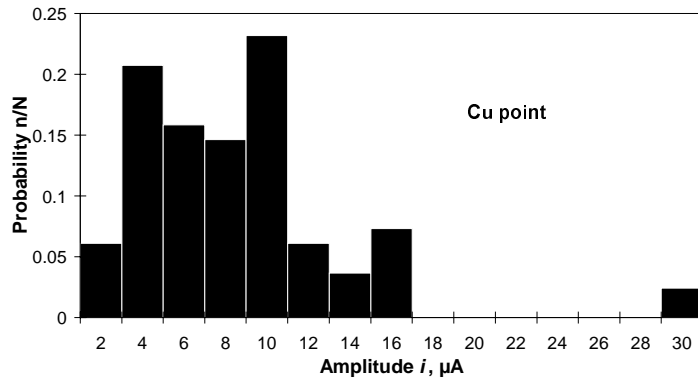**Figure 44.** Amplitude distribution of first current spikes.
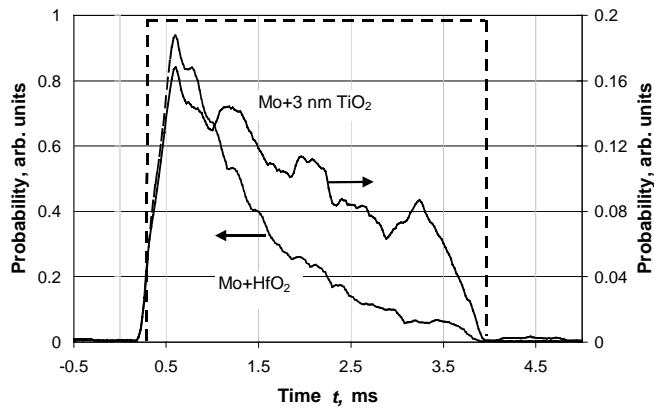
Figure 45. Probability of the rise of first current spike; dashed line — UV pulse.
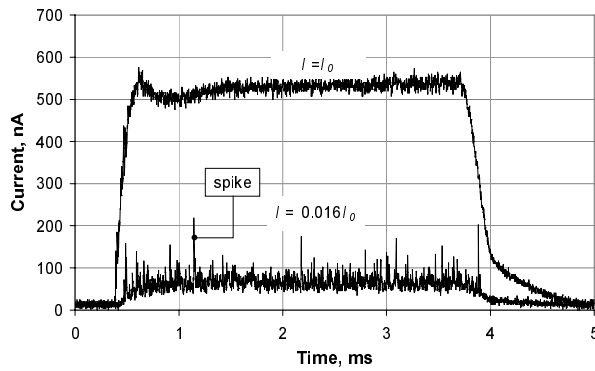
Figure 46. Influence of plateau current to spikes; Pt point; stressed plane, $U = 12.5$ kV.

56
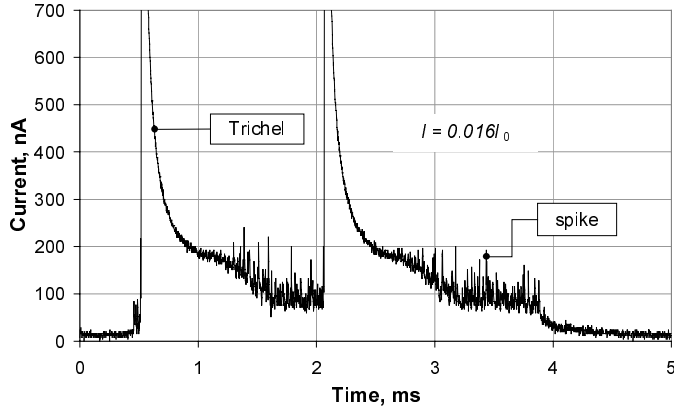
Figure 47. Steady component, spikes and Trichel pulses induced by UV pulse of low intensity; Pt point; stressed plane, $U = 12.6$ kV.

The dependence in Figure 47 is recorded at the voltage which is by 100 V higher than it was for data in Figure 46. When the value of the plateau current is small, a number of Trichel pulses could rise during UV pulse. The maximum number of Trichel arising during UV pulse is determined by the drift time of negative ions (Figure 26). At the same voltage the growth of UV intensity increases the plateau current. A result is that only one Trichel pulse arises and it starts already at very low instantaneous values of UV radiation.

The distribution function of the time interval between the beginning of UV pulse and beginning of Trichel pulse [7 (**Paper I),** Figure 15] is very similar to the same distribution for spikes (Figure 44). It was supposed, [7], that current spike triggers Trichel pulse. Indeed, Figure 48 demonstrates that Trichel pulse is preceded by spike. The time interval between the closest spike and Trichel pulse, t_{ST}, as well as the height of the spike, i_S, varied in large limits and the correlation coefficient between them was not high (Figure 49). Nevertheless, it is remarkable that the corresponding trendline follows the dependence $t_{ST} \propto i_S^{-1}$.

57
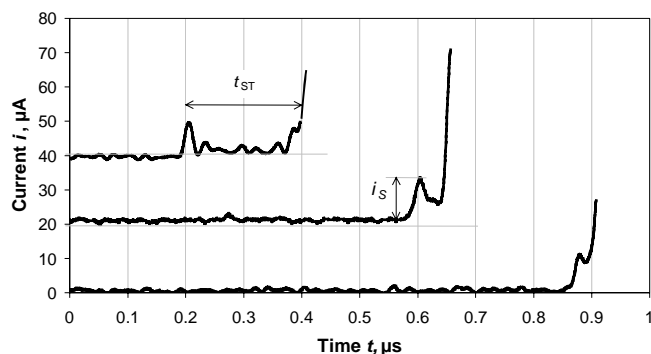
Figure 48. Spike-Trichel pulse sequence; Cu point; UV intensity $I = I_0$; stressed plane, $U = 14$ kV.
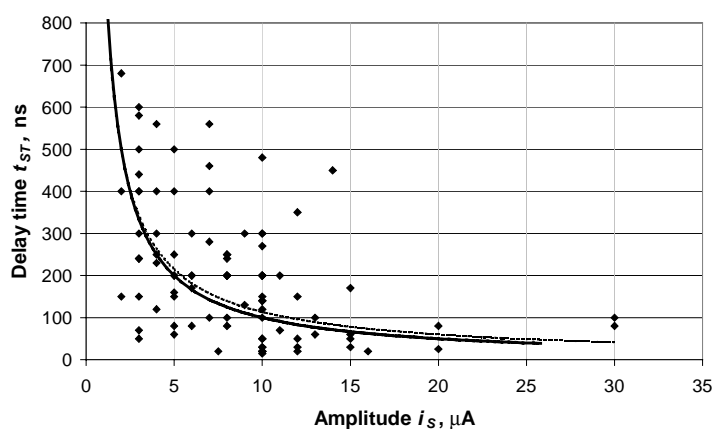
Figure 49. Delay time versus height of the spike; trendline is dashed, solid line follows the dependence $t_{ST} \propto i_S^{-1}$.

6.3.4. Characteristics of Trichel pulse

As it was mentioned in chapter 2 the onset potential of the spontaneous Trichel pulses does not depend on the point material. On the contrary, the inception voltages of UV-triggered Trichel pulses depend on the electrode material and the electrode coating.

Table 3 includes data of the inception voltages for different point types. Trichel pulses were triggered by pulsed UV radiation at the intensity $I = I_0$. [85] presented a similar table for the intensity $I = 0.016I_0$. Very different values of

the plateau current, i_{Pl}, correspond to the inception voltages, but any correlation between i_{Pl} and the inception voltage is missing. The result is not surprising as at larger currents of the plateau Trichel pulse arises preferably at the very beginning of UV pulse i.e. at a low instantaneous value of UV intensity (Subsection 6.3.3). At the same time there is an obvious correlation between the inception voltage and the electrode coating; as a rule the coating diminishes the inception voltage. The only exception is 70 nm TiO_2 coating.

Table 3

Point type	Inception voltage, kV stressed plane,	Plateau current, nA
Pt	12.6	500…850
Pt + C	12.0	7…9
Cu	13.9	325
Cu + C	12.0	10
Cu + CuI	13.7	640…760
Mo	13.5	<1
Mo + 1 nm TiO_2	13.0	70…110
Mo + 70 nm TiO_2	13.7	8
Mo + 3 nm HfO_2	13.1	26…80

Figures 50–54 present waveforms of Trichel pulses, which were recorded using preamplifiers of different sensitivities and bandwidth. Usually only the most intensive parts of the current pulse are recorded like in Figure 50. For repetitive Trichel pulses in the similar discharge gap the current peak had value of 6 mA while the current decay followed the same temporal dependence [86]. In Figure 51 there is the leading edge of the same pulse as in Figure 50 but it is presented in the linear time scale. The duration of the step is ≈ 0.5 ns. Before the step the current growth is faster than exponential, later the current increase slows down. At the same voltage the extent how pronounced the step was, varied from pulse to pulse. Similarly, the current peak of Trichel pulse varied during different recordings in the range of few milliamps.
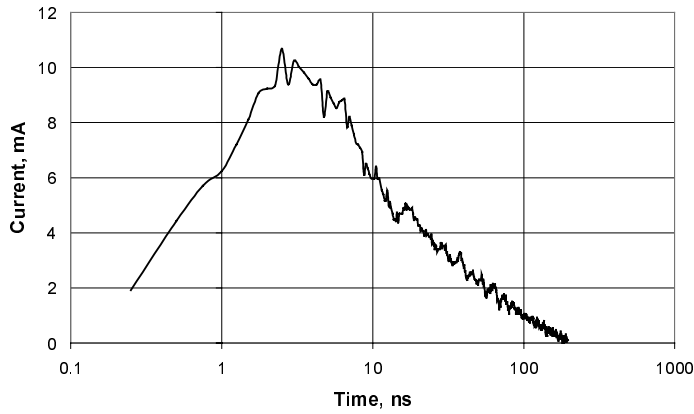
Figure 50 . Trichel pulse; aged Cu point; stressed plane, $U = 14.2$ kV; $I = 0.03$ I_0.
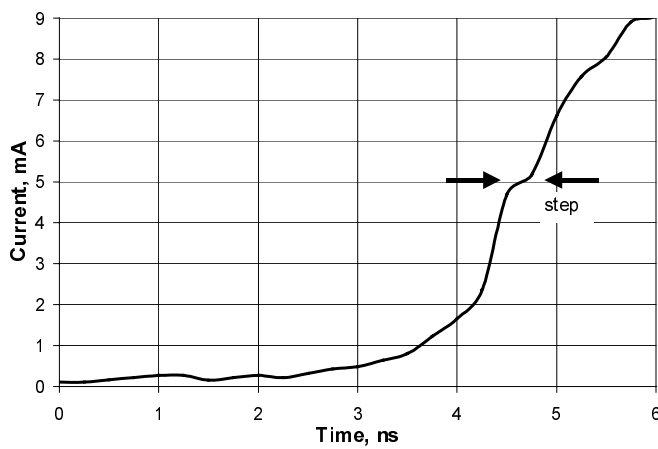
Figure 51. Leading edge of Trichel pulse; aged Cu point; stressed plane, $U = 14.2$ kV; $I = 0.03$ I_0.

Actually the current of Trichel pulse lasts during much longer time interval than it follows from Figure 50. Figure 52 brings out two characteristic regions on the time scale where the current decay fastens. The positions of these regions vary from pulse to pulse but the shifts occur conjointly. These characteristic regions were more or less pronounced for all points tested and they appear at the moments, which are close to those in Figure 52.

60
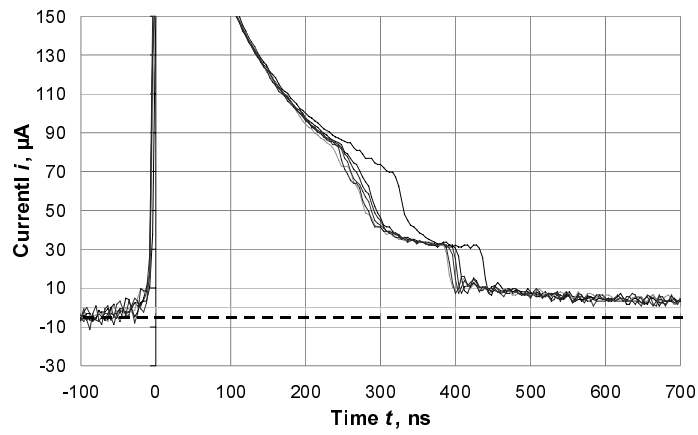
Figure 52. Decay of Trichel pulse; waveforms of six pulses; Cu + C point; stressed point, $U = 13.8$kV; $I = 0.016I_0$.

Further current decay is smooth and the total duration of the current pulse is ≈ 1 ms (Figures 53, 54). The latter is close to the calculated drift time of negative ions, t_d, in the gap (Figure 11).
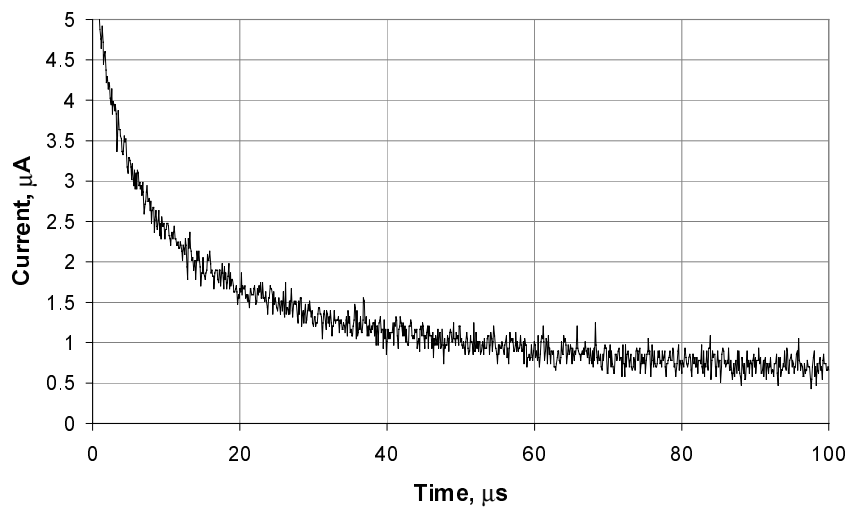
Figure 53. Mo + 3 nm HfO$_2$ point; stressed point, $U = 13.8$kV; $I = 1$.

61
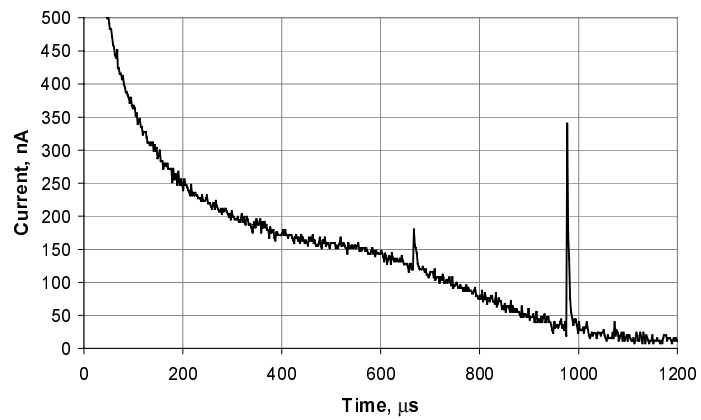
Figure 54. Pt point; stressed point, $U = 12.6$ kV; $I = 1/64$.

7. MODEL OF EMISSION AND CONCLUSIONS

As it appeared from previous chapters there are many factors influencing the rise of Trichel pulse. Indeed, one could trigger Trichel pulses both by ions and UV radiation. In the case of UV initiation we observed non-linear effects, it means that the explanation of the regularities only by some one-step emission process is impossible. Besides, even the low current mode had a complicated structure influenced by UV radiation. The regularities were the simplest in the case of the steady component of LCM. Furthermore, in this case we achieved the best reproducibility of measurements and there were no temporal limitations from the side of the recording system.

The aforecited factors were the reason why we used the data of the steady component of LCM for the setting of the emission model [84 (**Paper III**)]. Later the conclusions of the model are compared with the experimental findings.

7.1. Model of emission

At first glance sub-linear dependencies of the plateau current, i_{Pl}, on UV intensity, I, (Figure 41) could be caused by the space-charge effects of negative ions drifting in the discharge gap. In this case the effect of the current saturation must be more pronounced for points of larger currents. At the same time $i_{Pl} = f(U)$ dependencies for points having considerably different current values (Figure 55) practically coincide. This fact forces to overrule the assumption that the processes in the discharge gap control the current.
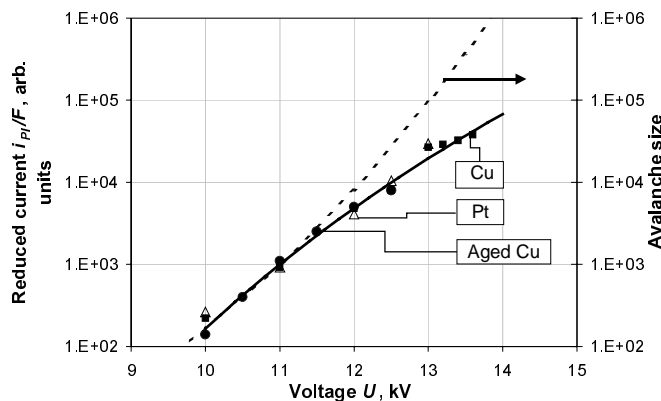
Figure 55. Reduced current i_{Pl}/F and calculated number of electrons in an avalanche versus applied voltage; factors F for Pt, fresh Cu and aged Cu are related as 8/2/1; UV intensity I has a fixed value; solid line — FN dependence fitted with experimental points.

In [59 (**Paper II**)] we tried to explain the non-linear dependence $i_{Pl} = f(I)$ by the accumulation of positive ions at the point surface. A layer of positive charge at the point surface should reduce the field in the ionisation zone. Indeed, an estimation gave a similar dependence of the plateau current on UV intensity like the experiment did (**Paper II,** Figure 1). However, more careful calculations forced to reject the assumption.

Finally we supposed that the observed saturation trends of the photo-induced current are related to the properties of the cathode emissivity. Extra assumption was that non-metallic inclusions at the point surface have a decisive role in the emission mechanism. Indeed, the principal differences between the dependencies for specially coated and non-coated points were missing. Furthermore, even in the case of Pt point the discharge started from the region of the point electrode where non-metallic microinclusions were embedded (Figure 9).

There is much in common in the initial stages of discharges in vacuum and high-pressure gas [46]. In vacuum, the experiments affirm the model of emission, which assumes the existence of non-metallic inclusions at the electrode surface (subsections 2.5.2, 2.5.3). On the ground of the above-mentioned circumstances we describe the emission according to the sketch in Figure 56. The sketch is close to that used for the explanation of the emission in vacuum (Figures 5, 6). The sketch should give the metal-insulator-gas band structure established after the conditioning procedure.
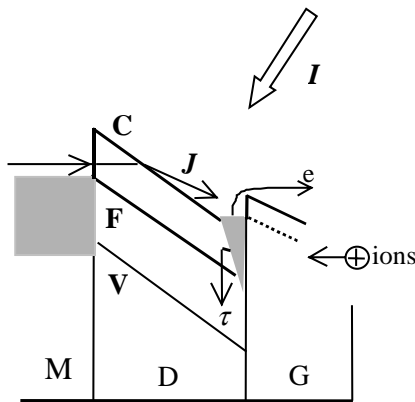
Figure 56. Model of photoinduced emission in the case of metal (M)-dielectric (D)-gas (G) structure; V — valence band; C — conduction band; F — Fermi level; other symbols are explained in the text.

According to Figure 56 the photons transfer the first electrons, e, into gas from a reservoir of a finite capacity at the dielectric-gas (DG) interface. The number of electrons emitted per second is proportional to UV intensity, I, and the amount of electrons, N_R, in the reservoir. If γ is the probability that a photon

liberates an electron from the reservoir, then $\gamma N_R I$ is the number of electrons emitted per time unit, i.e. it is the frequency ν (s^{-1}) of avalanches. Therefore the electron component of the current is

$$i_e = e\gamma N_R I \exp\left(\int \alpha_{eff} dx\right) \quad (1),$$

where e is elementary charge.

The number of electrons in the reservoir, N_R, changes with time. The reservoir is filled with electrons tunnelling through MD barrier (flux J). The amount of the electrons in the reservoir N_R diminishes due to the photo-induced emission (rate $\gamma N_R I$), the recombination of electrons with a part β of the positive ions created by the discharge avalanches (rate $\beta \gamma N_R I \exp\left(\int \alpha_{eff} dx\right)$), and other losses (time constant τ). Thus, the rate equation for the electrons in the reservoir is

$$\frac{dN_R}{dt} = J - \frac{N_R}{\tau} - \gamma N_R I\left[1 + \beta \exp\left(\int \alpha_{eff} dx\right)\right] \quad (2)$$

As it follows from (2), at the initial moment (i.e. $I = 0$) the amount of the electrons in the reservoir is $N_R(0) = J\tau$, and at the current plateau

$$N_R = \frac{J\tau}{1 + \gamma\tau I\left(1 + \beta \exp\left(\int \alpha_{eff} dx\right)\right)} \quad (3).$$

7.2. Current of LCM

In this section the calculated values of $\exp\left(\int \alpha_{eff} dx\right)$ (Figure 13) are used and it is set that the arbitrary UV intensity, I_0, corresponds to the photon flux 10^{10} s^{-1}. The latter value results from the estimation in section 3.4.

Replacing N_R in (1) by the expression (3) and assuming that $\beta \exp\left(\int \alpha_{eff} dx\right) \gg 1$ give for the plateau current

$$i_{Pl} = KeJ \frac{\gamma\tau I \exp\left(\int \alpha_{eff} dx\right)}{1 + \gamma\tau\beta I \exp\left(\int \alpha_{eff} dx\right)} \quad (4).$$

The order of magnitude of the factor K in (4) is one and it takes into account the percentage of the ion components in the plateau current. The relationship (4) was fitted with the experimental dependencies varying $\gamma\tau$, β and J. Actually the listed variables are not independent, i.e. if the value of one variable is fixed, it is possible to change the others in the limits less than 20%. Figures 41, 42 confirm that the model describes properly the dependence of the plateau current,

65

i_{Pl}, both on the intensity and voltage. Dashed straight lines in Figure 41 present the results of the calculations when we neglected the second term in the denominator of the expression (4).

For a certain point type, β has a fixed value, which does not depend on voltage: in the case of Cu + CuI point, β was close to one and for Cu + 3 nm HfO$_2$ point it was ten times smaller. For the same mentioned point types the fluxes J differ by two orders of magnitude (at $U = 12.5$ kV 5×10^{12} and 5×10^{10} s^{-1}, respectively) and they are voltage-dependent. The latter result is not surprising, as the emission through MD barrier follows the same Fowler-Nordheim (FN) type regularities like in the case of field emission from metals. The height of the barrier of MD interface is considerably lower than that for metals as it equals to the difference of the work function of the metal and the affinity of the dielectric. According to [87], the flux could be presented as

$$J = AV \exp\left(-\frac{B}{\sqrt{V}} \right) \tag{5},$$

where V is the voltage drop at the dielectric layer and the values of A and B depend on electrical properties of the dielectric. We assumed that the voltage drop V is proportional to the voltage U applied to the gap, and varying A and B we fitted the relationship (5) with the experimental results. Figure 55 demonstrates that FN dependence is close to the experimental one.

The value of the product $\gamma\tau$ was almost the same ($\approx 10^{-14}$ s) for all points tested. This, a little bit unexpected result should indicate that at atmospheric pressures both the emission probability γ and the time constant of losses τ are determined by the surrounding gas medium. From the latter conclusion follows that the role of the reservoir is played by the surface states of DG interface, the structure of which is determined by gas absorbed at the point surface [88].

In order to find the temporal changes of the photo-induced current, first the equation (2) was solved numerically and then the time-dependent frequency of the avalanches $v(t) = \gamma N_R(t)I(t)$ was calculated. If the frequency $v(t)$ and the waveform of a single avalanche are known, it is possible to calculate the photo-induced current. The true waveform of the avalanche current is the sum of its components, presented in Figure 14. Because of the limited bandwidth of the recording system the waveform of the avalanche deforms and at the screen of the oscilloscope a signal should appear like it is presented in Figure 57.
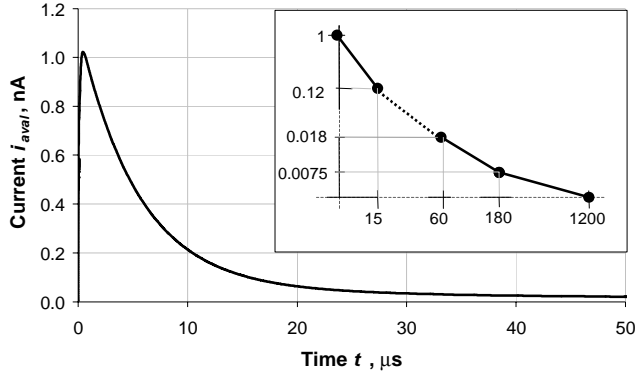
Figure 57. Calculated waveform of avalanche current as it could be recorded after passing the circuit of 5 μs time constant; $U = 13$ kV; inset — approximation of the avalanche current.

To reduce the computing time, the avalanche waveform was approximated by straight lines (Figure 57, inset) and the photo-induced current was found as

$$i(t) = \sum_n v(n\Delta t) i_{aval}(t - n\Delta t) \tag{6}.$$

In calculations was set $\Delta t = 1$ μs and $n = 4000$.

The measured and calculated curves in Figures 39, 40 are very close i.e. the model describes properly the main features of the photo-induced discharge. When fitting the calculation results with the recorded temporal changes of the current it was possible to determine the parameters γ and τ separately, the time constant of losses for the curves in Figure 40 is ≈ 200 μs.

The results of the calculations allow to interpret the regularities of the recorded current waveforms. The fast rise of the current (Figure 39) is mainly caused by the movement of positive ions and electrons in a high electric field near the point electrode, while the slow rise of ≈ 1 ms duration reflects the drift of the negative ions in the low field region. The current reaches its plateau when the negative ions arrive at the plane electrode. When the illumination of the point stops, the positive ions are quickly removed from the gap and the electrons are attached, these events cause the fast fall of the current, but the negative ions continue their drift towards the plane electrode. The drift of the negative ions is the reason why the current is recorded after the end of the light pulse. There is a remarkably large contribution ($\approx 30\%$) of the negative ion component to the total current.

The reason for the current overshot in Figure 40 is that at the initial moment the amount of electrons penetrating MD barrier is not able to balance the number of electrons leaving the reservoir, and N_R diminishes from the initial value,

67

$J\tau$, to a new equilibrium value. This new equilibrium value corresponding to the current plateau depends both on the voltage, V, and intensity, I.
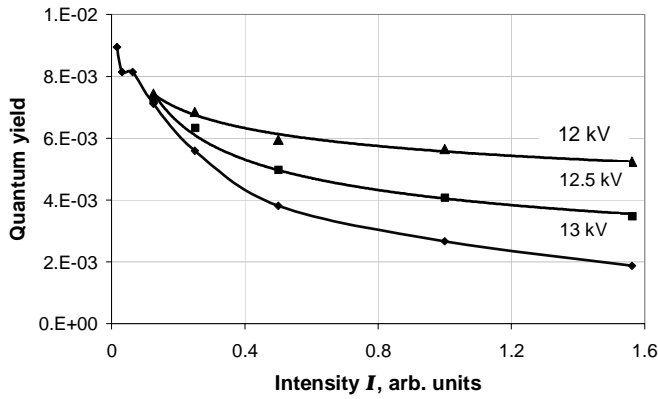
Figure 58. Quantum yield at the current plateau as a function of intensity at three different voltages; aged Cu point.

The product γN_R has the meaning of quantum yield, i.e. it characterises how many electrons per photon are liberated from the electrode. As N_R is a function of time, the quantum yield is also time depending. In the case of the discharge triggering by a short UV pulse, the value of the quantum yield should be considerably larger than that for steady UV triggering. Besides, Figure 58 demonstrates that the value of the quantum yield at the highest voltage used changes with the intensity growth more than four times. In spite of a large uncertainty of the estimation of the photon flux these numerical values of the quantum yield are rather close to those given in the literature [19].

7.3. Meaning of conditioning

The purpose of this section is to match experimental results presented in section 6.1 with the proposed emission model.

Under steady UV radiation the establishment of a stationary value of the discharge current could last several minutes. For this reason it has sense to connect the conditioning only with the changes occurring in the band structure of the electrode (Figure 56). We assume that in gases the band structure, MDG, passes during the conditioning the same steps like the band structure in vacuum, MDV, does.

In the case of vacuum emission (Figures 5, 6) the band bending is caused by the filling of surface states at the dielectric-vacuum interface. The filling is

achieved due to the increase of the voltage drop at MDV structure. The similar bending of bands should also occur in case the third component of the structure is gas. Compared with vacuum, the main difference is that the voltage growth is not the only reason of the filling. First, in experiments the voltage was changed in a very limited range and, secondly, at a fixed voltage UV radiation causes considerable time-depending growth of the current (Figure 30). There is a correlation between the band gaps of the coating materials and the recorded current values. Indeed, the currents for points with TiO_2 and HfO_2 coatings of the same thickness differ considerably (Figure 34). So, it seems that during the conditioning UV photons transfer the electrons to the surface states from the valence band. In other words, the role of UV radiation is similar to the voltage increment. Once established, MDG maintains its structure during a very long time interval (Figure 31).

The final value of the photo-induced current could be larger or smaller than it is at the moment of UV switch-on (Figure 29). Obviously, the result depends on the competition between the charging and discharging (section 7.1, (2)) of the reservoir, the reasons of both processes are connected with UV radiation.

The current dependence on airflow lasts during a long time interval (Figure 27). It should point that gas layers absorbed at the point surface have a large influence to the surface states.

The current has a strong dependence on temperature (Figure 28). One of the explanations could be that the temperature change alters the absorption/desorption equilibrium of the gas thus influencing surface states.

7.4. Speculations concerning spikes and Trichel pulses

According to the results of section 7.2 the emission model proposed works. The question is, could the model explain the experimental findings related with the current spike of LCM and Trichel pulse.

Spikes are added to the steady component of LCM due to the voltage increment. As the spike characteristics differ considerably from those of the steady component, the spike appearance should be connected with some changes of MDG structure (Figure 56). In vacuum an explosive-like growth of emission is caused by the lowering of the height of DV barrier (Figure 6, transition from step 2 to step 3). Let us assume that a similar change is the reason of the spike appearance. In this case the solid line indicating the height of DG barrier in Figure 56 should be replaced by the dashed line. It means that electrons in the reservoir become 'hot' and no external help is needed for their emission.
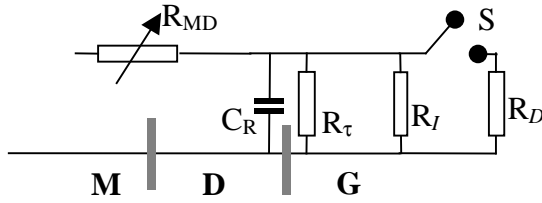
Figure 59. Electrotechnical circuit replacing MDG structure in the case the emission of hot electrons becomes possible. Symbols are explained in the text.

For further comparison of experimental findings and the emission model we replaced MDG structure by a simple electrotechnical circuit (Figure 59). In the figure MD barrier is replaced by a non-linear resistor R_{MD}, the resistance of which depends on the voltage drop, V, at MDG structure. Electron reservoir at DG is presented as a capacitor C_R, which have leak (resistor R_τ). When the point electrode is illuminated, an extra resistor, R_I, is switched to the capacitor. The capacitor is charged by electrons penetrating MD barrier, and discharged through $R_\tau$ and R_I. The position of the switch, S, depends on the charge in the capacitor. At a certain value of the charge the switch closes and the capacitor discharges with the time constant $C_R R_D$. The burst of emitted electrons gives the beginning of the current spike. In addition to the applied voltage, the appearance of spikes depended on the UV intensity, at higher values of the intensity the spikes did not rise (Figure 46). The finding matches with the model. Indeed, as $R_I \propto I^{-1}$, the charge in the capacitor may never reach the value needed for closing of the switch, S.

At the inception voltage the spikes and Trichel pulses coexist and the rise of Trichel pulse is related with the preceding spike (Figures 48, 49). The time intervals between the spike and Trichel pulse were big compared with the drift time of positive ions in the gap. So, the triggering effect of spikes could be explained only by the accumulation of spike-created positive ions at the point surface. The similar effect of accumulation explains the finding in section 5.2 where the repetition rate of Trichel pulses did not depend on if the flux of triggering ions had pulsed or steady manner. The accumulation of ions at the point surface could change the voltage drop at MGD structure. The last assumption is supported by a linear dependence presented in Figure 18.

An enlargement of the voltage drop at MGD structure causes further lowering of DG barrier and a considerably larger burst of electrons is emitted i.e. Trichel pulse arises. As $R_I \propto I^{-1}$, UV intensity should have the same influence on Trichel pulses like it had in the case of spikes. Indeed, the growth

70

of UV intensity suppresses Trichel pulses (Figure 24), thus shifting the inception voltage towards its higher values (Figure 35).
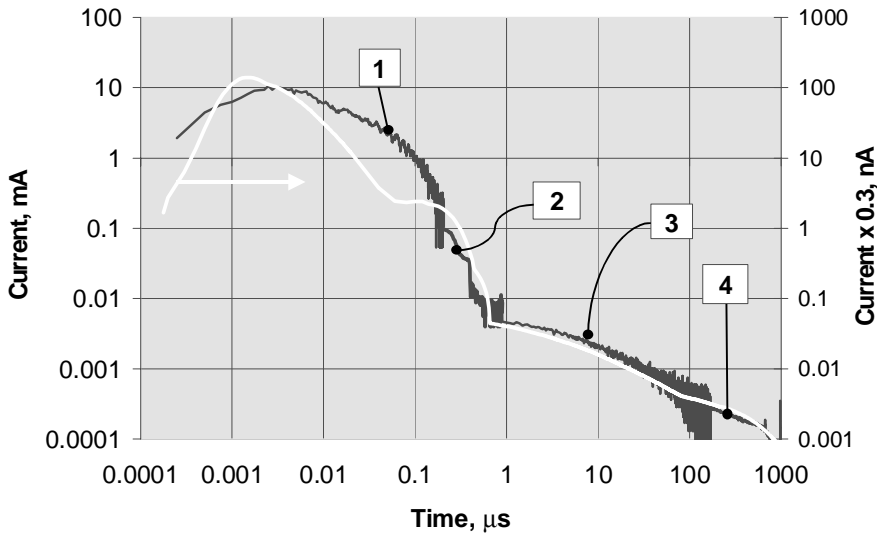
Figure 60. White — waveform of the avalanche calculated for $U = 13$ kV, stressed point; black — measured waveforms of Trichel pulse; further explanations in the text.

Although no contradiction between the model and experimental results was found, the description of the phenomena was totally qualitative. Some quantitative data could be obtained comparing the waveform of Trichel pulse with that of the avalanche.

Figure 60 compares the current of Trichel pulse with the current of an avalanche. In the figure the calculated waveform of the avalanche current is simply the sum of the current components presented in Figure 14. The measured current waveform was compiled of the dependencies in Figures 50, 52–54 (parts 1–4, respectively). It should be pointed that the parts of the experimental curve belong to different recordings. Furthermore, the point electrodes as well as applied voltages were different. It means that for a certain time moment the current values may differ by 20%. The last-accounted reasons give the basis to estimate the coincidence of the curves in the current-scale as a good one. Thus it is possible to estimate that at the start of Trichel pulse approximately 10^4 avalanches develop.

Examining the temporal changes it is easy to distinguish the regions where the different current components are dominating. In region 1 the electron component is dominating; region 2 reflects the drift of positive ions, and 3, 4, the movement of negative ions. The difference is the largest between the electron components and this demands a special study.

71

As the first approximation let us assume that the electron emission follows an exponential decay characteristic to the discharge of the capacitor, C_R, in Figure 59. If the frequency of avalanches is set then assuming Laplacian field distribution it is possible to find the corresponding current as it was done earlier (relationship (6), section 7.2). The electron component of the current was calculated setting the time step $\Delta t = 0.1$ ns. Figure 61 compares the calculated waveform and Trichel pulse. In calculations the decay time of emission was characterised by the value of 3.5 ns.
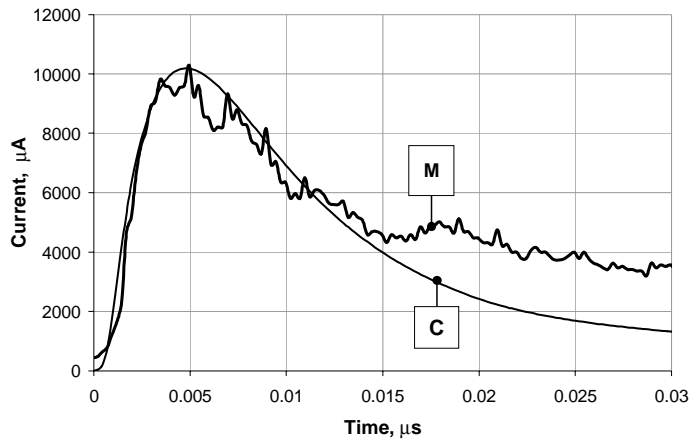
Figure 61. Measured Trichel pulse (M) versus calculated waveform (C).

Bearing in mind how simple the starting considerations of the calculations were, the coincidence could be estimated as a good one. Of course, the calculated curve does not follow the temporal changes at the leading edge but it is not the main task of the present calculations. More important is the result that the essential discrepancy between the curves appears only for times larger than 15 ns. It means that till this moment the field distortion by ion space charges plays a negligible role.

It seems that our results are closest to the considerations that form the basis of the modelling presented in [28, 29]. Similarly to our studies the electron emission follows FN type of dependence that depends on time. Besides, like in our case, it seems that during the first ten nanoseconds of Trichel pulse development the feedback from the discharge side has a negligible influence on the emission. However, in these studies the field enhancement factor was introduced to achieve the field strength needed for an efficient FN emission from metals. In our model where the emission is governed by the tunnelling through metal-dielectric interface the field strength needed is considerably lower.

72

7.5. Open problems

In the previous sections of the chapter no contradictions between the model and experiment were found. Nevertheless, there are a number of open problems, demanding further studies.

- It was supposed (section 7.2) that the product $\gamma\tau$ is determined by the gas composition. Unfortunately, it is only an assumption. In order to verify the assumption, measurements should be done in the gas medium of more determined composition than it is air. Adding to the main gas some additives (like O_2, CO_2 etc) and recording dependencies like in Figure 40 should prove/overrule the assumption.

- As it was found, the conditioning procedure prepares MDG structure. Using different ways of conditioning, the parameters of the emitted burst of electrons should alter and the waveform of Trichel pulse should reflect the change.

- The experiments were carried out with spectrally unresolved UV radiation. It was supposed that the radiation is responsible both for the charging and discharging of surface states. At the same time it is hardly possible that the value of the energy gap and the height of DG barrier coincide. So it is possible that photons ensuring the filling of surface states belong to other spectral region than photons causing the electron emission. Only spectral measurements could clarify the actual situation.

- The model brings to the foreground the properties of MD barrier. In this case the third component of the electrode structure should have a minor role. Consequently, some regularities (like long-term memory effects) of metal-dielectric-metal structure should be close to those observed in the case of MDG structure. It is comparatively easy to check the assumption carrying out parallel studies with layers of the same composition and thickness.

73

8. SUMMARY

The paper presents the results of experimental and theoretical study of the low current mode of negative corona. The purpose of the study was to find the electron emission mechanism that is responsible for the rise of negative corona pulses.

The main idea of the study based on earlier observations that the presence of non-metallic inclusion at the electrode favours the rise of negative corona discharge. For this reason a systematic study of negative corona was carried out also with electrodes, which had coatings of known composition and thickness.

The development of the conditioning procedure as well as the reliable technique of the external triggering of the discharge allowed achieving results of good reproducibility.

Recording devices elaborated, recorded the discharge current in the range of 10^{-10}–10^{-2} A with an adequate time resolution.

As it appeared from the study of the non-self-sustained UV triggered discharge, the electrodes made of different substrate materials or coatings have quantum yields of photoemission, the values of which differ considerably. Thin dielectric coatings may increase the yield by many orders of magnitude. Besides, the quantum yield was a non-linear function of UV intensity and it changes with time.

In order to calculate the discharge parameters in the gas medium the modelled electric field distribution was used. In calculations the most straightforward computing algorithms were applied.

Equations describing the emission were composed on the basis of processes occurring at the metal-dielectric-gas structure. It was assumed that the emission takes place from the reservoir of a finite capacity situating at the dielectric-gas interface. The reservoir is filled by electrons penetrating metal-dielectric interface i.e. at this interface there occurs Fowler-Nordheim type of emission. Thus the amount of electrons in the reservoir is time-depending interplay between the charging-discharging of the reservoir. For this reason the quantum yield is also time-depending and it changes with UV intensity.

The dependencies that followed from the model fit with the experimental findings.

The results of the study confirm that the rise of negative corona is controlled by Fowler-Nordheim type of emission, which occurs at the metal-dielectric interface.

SUMMARY IN ESTONIAN

Negatiivse koroonalahenduse nõrga voolu staadium

Käesoleva töö temaatika kuulub madalatemperatuurilise mittestatsionaarse plasma valdkonda. Koroonalahenduse huviobjektiks on ionisatsiooninähtused tugevasti mittehomogeenses elektriväljas. Sellisel juhul on gaasi ionisatsioon ja ergastamine koondunud ühe elektroodi juurde. Kui see elektrood omab negatiivset polaarsust, siis kõneldakse negatiivsest koroonalahendusest.

Peale akadeemilise huvi seonduvad koroonalahenduse uurimisega mitmed praktilised rakendused. Olulise näitena võib tuua gaaslahendusplasmat töökeskkonnana kasutavad laserid, mille üheks väljundparameetreid piiravaks faktoriks on ionisatsioonilised ebastabiilsused. Oma algstaadiumides on elektroodilähedase ionisatsioonilise ebastabiilsuse kulg vähe sõltuv elektrivälja jaotusest. Kuna koroonalahenduse puhul on objekt ruumiliselt paremini lokaliseeritud ja plasma tagasimõju on oluliselt väiksem, lubavad koroona uuringud saada tulemusi, mis on rakendatavad plasmafüüsika laias valdkonnas.

Koroonalahenduse uurimisel on lähiajal üheks erutavamaks probleemiks põhjuste väljaselgitamine, miks kasvab vool mõne nanosekundi jooksul kuni üheksa suurusjärku. Voolu kasvu kohta viimase paari suurusjärgu piires on kogutud usaldusväärne eksperimentaalne materjal ning lahenduse modelleerimisel saadud tulemusi võrreldakse just nende andmetega. Erinevad mudelid eeldavad põhimõtteliselt erinevaid algelektronide emissiooni-mehhanisme, kuid lähteparameetrite mõningase varieerimise tulemusena saadakse eksperimendiga ligilähedane tulemus. Kuna eksperimentaalne teave lahendusest nõrgematel vooludel on napp, puuduvad ka kriteeriumid erinevate mudelite usaldusväärsuse hindamiseks.

Käesoleva töö eesmärgiks on eksperimentaalse teave hankimine koroonalahenduse nõrga voolu moodist ning saadud tulemuste põhjal voolu hüppelist kasvu kirjeldava emissioonimudeli väljatöötamine.

Eksperimendis kasutati koroonalahendusele tavapärast teravik-plaat lahendusvahemikku. Töökeskkonnaks oli tolmuvaba atmosfäärirõhul õhk, kus koroonalahendus eksisteerib impulsside (Tricheli impulsid) kujul. Varasematest uuringutest oli teada, et koroonalahenduse teket hõlbustavad oluliselt katoodi pinnal leiduvad mittejuhtivad lisandid. Nende lisandite omadused on tavaliselt raskesti kontrollitavad. Käesoleva töö esmaseks uudseks momendiks oli teravik-elektroodi katmine kiledega, mille omadused olid teada. Teiseks õnnestus välja töötada koroonalahenduse välise käivituse meetodid kasutades positiivsete ioonide voogu ja/või ultraviolettkiirgust. Töös väljatöötatud mõõtetehnika lubas registreerida lahedusvoole kaheksa suurusjärgu piires, kusjuures oli garanteeritud protsesside kulgemiskiirusele vastav ajaline lahutus.

75

Elektrivälja jaotus lahendusvahemikus modelleeriti ning selle alusel leiti lahenduse kulgu gaasikeskkonnas määravad suurused (ionisatsiooniintegraal, triivikiirused jne). Lisaks sellele arvutati laengukandjate laviini poolt välisahelas indutseeritud vooluimpulss. Anti numbriline hinnang koroonalahenduse eksisteerimise piirkonnale, milles tuleb arvestada negatiivsete ioonide ruumlaengu pärssivat mõju emissioonile.

Detailselt uuriti nõrga voolu lahenduse sõltuvust elektroodi pinnakatte tüübist, initsieeriva ultraviolettkiirguse intensiivsusest, lahendusvahemikule rakendatud pingest ja ajast. Esmaseks uudseks leiuks oli, et atmosfäärirõhul ja õhus sõltub emissiooni fotosaagis tugevasti nii katoodi materjalist kui ka kattekile tüübist ja paksusest. Teiseks selgus, et fotovool sõltub initsieeriva kiirguse intensiivsusest mittelineaarselt ning konstantsel intensiivsusel on fotovool funktsioon ajast.

Nõrga voolu mood omab Tricheli impulsi lävele lähedastel pingetel keerulist struktuuri, tema otseselt ultraviolettkiirgusega seonduvale komponendile lisanduvad lühiajalised (ca 10 ns) impulsid mille amplituud on suurusjärke suurem alaliskomponendist. Mõõtmist johtus, et just nende impulssidega korreleerub Tricheli impulsi teke.

Emissiooni kirjeldavate võrrandite koostamisel võeti aluseks metall-dielektrik-gaas struktuur. Oletati, et footonite toimel emiteeritakse elektronid lõpliku mahtuvusega reservuaarist, mis asetseb dielektrik-gaas siirdel. Reservuaar täitub Fowler-Nordheim tüüpi emissiooni tõttu läbi metall-dielektrik siirde. Sõltuvalt rakendatud pingest, kiirguse intensiivsusest ning ajast muutub ka elektronide hulk reservuaaris. Lõpptulemusena kajastub nimetatud muutus registreeritava voolu suuruses ja ajalises dünaamikas. Võrdlus eksperimendiga näitab, et mudel kirjeldab hästi nõrga voolu lahendusele iseloomulikke seoseid.

Töös tuuakse ka emissioonimudelil baseeruv, kuid poolkvalitatiivne, kirjeldus protsessidest, mis käivitavad Tricheli impulsi. Arvuline hinnang näitab, et ca 10^4 elektroni emissioon paari nanosekundi jooksul genereerib vooluimpulsi, mis esimese 15 ns kestel on lähedane eksperimendis registreeritud Tricheli impulsiga.

Töö põhitulemuseks on emissioonimudeli väljatöötamine. Mudelist selgub, et Fowler-Nordheimi tüüpi emissioon metall-dielektrik siirdel määrab ajas muutuva elektronide emissiooni gaasi.

REFERENCES

[1] Sigmond R S, Goldman M 1981 Corona Discharge Physics and Applications In: *Elec. Breakdown and Discharges in Gases* Les Arcs Part B N Y London NATO ASI Series B: Phys. **89B** 1–64

[2] Loeb L B 1965 *Electrical coronas* (Berkeley & Los Angeles) ch. 4

[3] Sigmond R S 1978 Corona Discharge In: *Electrical Breakdown in Gases* ed Meek J M and Craggs Wiley 319–384

[4] Weissler G L 1943 Positive and negative point-to-plane corona in pure and impure hydrogen, nitrogen and argon *Phys Rev.* **63** 96–107

[5] Miller C G, Loeb L B 1951 Negative Coaxial Corona Discharges in Pure N_2, O_2 and Mixtures Thereof *J. Appl. Phys.* **22** 614–621

[6] Korge H, Kudu K, Laan M 1979 The discharge in pure nitrogen at atmospheric pressure in point-to-plane discharge gap 3rd *Int. Symp. On High Voltage Engineering* (Milan) paper 31. 04

[7] Laan M, Paris P, Repän V 1997 Triggering of Negative Corona, *Inv. Pap. XXIII ICPIG* (Toulouse) France Journal de Physique IV, **7**, Col. C4 259–270

[8] Josepson R 2004 Negative corona in N_2+O_2 mixtures *MSc Thesis* University of Tartu

[9] Trichel G W 1938 The mechanism of the Negative Point to Plane Corona near Onset *Phys. Rev.* **54** 1078–1084

[10] Cross A, Morrow R, Haddad G N 1986 Negative point-plane corona in oxygen *J. Phys. D: Appl. Phys.* **19** 1007–1017

[11] Lama W L, Gallo C F 1974 Systematic study of the electrical characteristics of the "Trichel" current pulses from negative needle — to-plane coronas *J. Appl. Phys.* **45** 103–113

[12] Napartovich A P, Akishev Yu S, Deryugin A A, Kochetov I V, Pan'kin M V, Trushkin N I 1997 A numerical simulation of Trichel-pulse formation in a negative corona *J. Phys. D: Appl. Phys.* **30** 2726–2736

[13] Akishev Yu S, Grushin M E, Kochetov I V, Napartovich A P, Trushkin N I 1998 The establishment in time of Trichel pulses in negative pin-plane corona. A comparison of theory and experiment *ESCAMPIG 98* **22H** 168–169

[14] Aleksandrov G N 1956 Initial stages of negative corona *J. Technical Phys.* **26** 2633–2639 (in Russian)

[15] Morrow R 1985 Theory of negative corona in oxygen *Phys. Rev. A* **32** 1799–1809

[16] Zentner R 1970 Stufenimpulse der negativen Koronaentladung ETZ-A **91** 303–305

[17] Černák M, Hosokawa T, Kobayashi, Kaneda T 1998 S Streamer mechanism for negative corona current pulses *J. Appl. Phys.* **83** 5678–5690

[18] Morrow R 1985 Theory of stepped pulses in negative corona discharges *Phys. Rev. A* **32** 3821–3824

[19] Raizer Y P 1987 *Physics of Gas Discharges* (Moscow: Nauka) ch. **6** (in Russian)

[20] Černák M, Hosokawa T 1988 Similarities between the initial phase of a transient nonuniform glow discharge in nitrogen and the negative corona Trichel pulse formation in an electronegative gas *Appl. Phys. Lett.* **52** 185–187

[21] Černák M, Kaneda T, Hosokawa T 1989 First Negative Corona Pulses in 70% N_2 + 30% SF_6 Mixture *Japanese Journal of Applied Physics* **28** 1989–1996

[22] Černák M, Hosokawa T 1989 Secondary electron emission in the course of the first Trichel-like pulse development in N_2+SF_6 mixtures *IEEE Transactions of Electrical Insulation* **24** 699–708

[23] Černák M, Hosokawa T 1991 Complex form of current pulses in negative corona discharges *Phys. Rev. A* **43** 1107–1109

[24] Černák M, Hosokawa T 1992 Negative Corona Current Pulses and Cathode Sheath Instabilities in a Short Point-Plane Gap in CO_2 *Aust. J. Phys.* **45** 193–219

[25] Torsethaugen K, Sigmond R S 1973 The Trichel pulse phase of negative coronas in the Trichel pulse regime in air 1973 *ICPIG XI* (Prague) *Contrib. Papers* 195

[26] Laan M, Perelygin V 1991 The dependence of negative corona on electrode surface properties *ICPIG XX* (Pisa, Italy) *Contrib. Papers* 929–930

[27] Gupta D K, Mahajan S, John P I 2000 Theory of step on leading edge of negative corona current pulse *J. Phys. D: Appl. Phys.* **33** 681–691

[28] Reess T, Paillol J 1997 The role of the field-effect emission in Trichel pulse development in air at atmospheric pressure *J. Phys. D: Appl. Phys.* **30** 3115–3122

[29] Paillol J, Espel P, Reess T, Gibert A, Domens P 2002 Negative corona in air at atmospheric pressure due to a voltage impulse *J. Appl. Phys.* **91** 5614–5621

[30] Raether H 1964 *Electron Avalanches and Breakdown in Gases* (London: Butterworths)

[31] English W N, Loeb L B 1949 Point-to-plane corona onsets *J. Appl. Phys.* **20** 707–711

[32] Bandel H W 1951 Point-to-plane corona in dry air *Phys. Rev.* **84** 92–99

[33] Korge H, Laan M, Paris P 1993 On the formation of negative corona *J. Phys. D: Appl. Phys* **26** 231–236

[34] Loeb L B, Kip A F, Hudson G G 1941 Pulses in negative point-to-plane corona *Phys. Rev.* **60** 714–722

[35] Laan M, Paris P, Perelygin V 1992 Laser action on corona pulses *Acta Phys. Slov.* **42** 91–97

[36] Paris P, Laan M, Tiirik A 1997 UV controlled repetition rate of Trichel pulses *ICPIG XXIII* (Toulouse) *Contr. Papers* **IV** 32–33

[37] Hosokawa T, Kondo Y, Miyoshi Y 1969 Prebreakdown Phenomena of Negative Point-to-Plane Air Gap *Electrical Engineering in Japan* **89** 120–127

[38] Fieux R, Boutteau M 1970 Phénomenes de prédécharges entre une pointe et un plan dans l'air sous tension continue *Bulletin de la Direction des Études et Recherches — E.D.F. — Serie B* **2** 55–88

[39] Golinski J, Grudzinski J 1986 Some properties of Trichel pulses with AC voltage *J. Phys. D: Appl. Phys.* **19** 1497–1505

[40] Hernandez-Avila J L, Nur M, Bonifaci N, Denat A 1995 D. C. Negative corona discharge characteristics in high density nitrogen in point-plane configuration *XXII ICPIG* (Hoboken, USA) *Contr. Papers 2* 129–130

[41] Dutton J 1978 Spark Breakdown in Uniform Fields In: *Electrical Breakdown in Gases* ed Meek J M and Craggs (Wiley) 209–318

[42] MacDonald A D 1966 *Microwave Breakdown in Gases* (New York: Wiley)

[43] Boyle W S, Kisliuk P 1955 Departure from Paschen's law of breakdown in gases *Phys. Rev.* **97** 255–259

[44] Koroliev Y D, Mesyats G A 1982 *Field and Explosive Processes in Gas Discharge*s (Novosibirsk: Nauka) (in Russian)

[45] Mesyats G A 1993 *Ectons* (Yekaterinburg: UIF Nauka) vol. **1, 2** (in Russian)

[46] Mesyats G A 1997 Ectons and their Role in Electrical Discharges in Vacuum and Gases *Inv. Pap. ICPIG XXII* (Toulouse, France) *Journal de Physique IV* **7** Col. **C4** 94–112

[47] Latham R V, Bayliss K H, Cox B M 1986 Spatially correlated breakdown events initiated by field electron emission in vacuum and high-pressure SF_6 *J. Phys. D: Appl. Phys.* **19** 219–231

[48] Latham R V 1981 Recent advances in the understanding of prebreakdown electron emission In: *High Voltage Vacuum Insulation: the Physical Basis* by Latham R V (London: Academic Press) 211–227

[49] Bayliss K H, Latham R V 1986 An analysis of field-induced hot-electron emission from metal-insulator microstructures on broad-area high-voltage electrodes *Proc. R. Soc. Lond.* **A403** 285–311

[50] Latham R V 1988 High Voltage Vacuum Insulation New Horizons *IEEE Trans Electrical Insulation* **23** 881–895

[51] Binh Vu T, Adessi Ch 2000 New Mechanism for Electron Emission from Planar Cold cathodes: The Solid State Field-Controlled Electron Emitter *Phys. Rev. Letters* **85** 864–867

[52] Binh Vu T, Sernet V, Dupin J P, Guillot D 2001 Recent progress in the characterization of electron emission from solid-state field-controlled emitters *J. Vac. Sci. Technol.* **B 19** 1044–1050

[53] Binh Vu T, Dupin J P, Adessi Ch, Sernet V 2000 Solid-state field-controlled emitters: a thin-film technology solution for industrial cathodes *Solid-State Electronics* **45** 1025–1031

[54] Aarik J, Aidla A, Uustare T, Sammelselg V 1995 Morphology and structure of TiO_2 thin films grown by atomic layer deposition *J. Crystal Growth* **148** 268

[55] Aarik J, Aidla A, Kiisler A, Uustare T, Sammelselg V 1999 Influence of substrate temperature on atomic layer growth and properties of HfO_2 thin films *Thin Solid Films* **340** 110–116

[56] Aarik J, Aidla A, Kiisler A, Uustare T, Sammelselg V 1997 Effect of crystal structure on optical properties of TiO_2 films grown by atomic layer deposition *Thin Solid Films* **305** 270–273

[57] Waldorf A J, Dobrowolski J A, Sullivan B T, Plante L M 1993 Optical coatings deposited by reactive ion planting *Applied optics* **32** 5583–5593

[58] Laan M, Repän V, Roos H 1994 Repetition rate of Trichel pulses and conditioning *Acta Physica Universitatis Comenianae* **35** 175–179

[59] Repän V, Laan M, Paris P, Aarik J, Sammelselg V 1999 Negative Coronas: Low Current Mode — Pulse Mode Transition *Czech. J. Phys.* **49** 217–224

[60] Samuila A, Dascalescu L, Mizuno A, Tobazéon R 1995 Effect of conductive particles on the dielectric strength of atmospheric air-caps in the presence of corona *11th Int. Conf. on Gas Discharges and Their Applications* **I** 140–143

[61] Gupta D K, Mahajan S, Kulkarni S V, John P I 1999 Effect of Dust Particles on Trichel Corona Discharge *ICPIG XXIV* (Warzaw) *Contr. Papers* **IV** 111–112

[62] Goldman A 1976 Effects de la décharge couronne négative sur des surfaces *Revue générale de l'électricité* **85** 679–680

[63] Tamm E, Mirme A, Kikas Ü 1992 Corona discharge as a generator of nanometer-range monodisperse aerosol In*: Air ions and electrical aerosol particles Acta Comment. Univ. Tartuensis* **947** 80–88

[64] Kikas Ü, Mirme A, Tamm E, Raunemaa T 1996 Statistical characteristics of aerosol in Baltic Sea region *J. Geophys. Res. Atmos.* **101/D14** 19319–19327

[65] Paris P, Laan M, Mirme A, Veldhuizen E M 1996 Corona discharge as generator of aerosol *HAKONE V* (Czech Rep., Milovy) *Contr. Papers* 185–189

[66] Laan M, Paris P, Repän V, Uustare 1994 T Laser triggered negative corona, *12th ESCAMPIG — European Sect. Conf. on the Atomic and Molecular Physics of Ionized Gases* (Noordwijkerhout, The Netherlands) *Inv. Lectures and Contr. Papers* 358–359

[67] *L2D2 lamps (deuterium lamps)*
http://www.hpk.co.jp/eng/products/ETD/pdf/L2D2_TLSO1027E05.pdf

[68] Houten v M A 1990 Electromagnetic compatibility in high-voltage engineering *Ph. D Thesis* Eindhoven University of Technology

[69] Repän V, Laan M, Plank T 2002 Electric field modeling for point-plane gap — *HAKONE VIII: Int. Symp. High Pressure Low Temperature Plasma Chemistry* (Tartu, Estonia) *Contrib. Papers* **P2.2** 134–138

[70] Zhou P 1993 *Numerical Analysis of Electromagnetic Fields* Berlin: Springer

[71] Kennedy J T 1995 Study of the avalanche to streamer transition in insulating gases *Ph. D Thesis* Eindhoven University of Technology

[72] Badaloni S, Gallimberti I 1972 *Basic data of air discharges* Upee-72/05

[73] Wen C, Wetzer J M 1989 Determination of swarm parameters in dry air with a fast timeresolvet swarm technique In: *Proc. XIX Int. Conf. Phenom. Ionized Gases* **3** 592

[74] Wen C 1989 Time resolved swarm studies in gases with emphasis on electron detachment and ion conversion *Ph. D Thesis* Eindhoven University of Technology

[75] Tammet H 1998 Reduction of air ion mobility to standard conditions *J. Geophys. Res.* **103** 13933–13937

[76] Luts A 1995 Evolution of negative small ions at enhanced ionization *J. Geophys. Res.* **100** 1487–1496

[77] Sigmond R S, Lågstad I H 1993 Mass and species transport in corona discharges *High Temp. Chem. Processes* **2** 221–229

[78] Sato N 1980 Discharge Current Induced by the Motion of Charged particles *J. Phys. D: Appl. Phys.* **13** L3–L6

[79] Sigmond R S 1997 The oscillations of the Positive Glow Corona *Inv. Pap. ICPIG XXII* (Toulouse, France) *Journal de Physique IV* **7** Col. **C4** 383–396

[80] Laan M, Paris P, Repän V 1997 Gas flow contra stagnant medium: changes of cathode emissivity in a point-plane gap *ESCAMPIG 13* (Poprad, Slovakia, 1996) Part B **20E** 431–432

[81] Davies A J, Evans C J, Llwewellyn Jones F 1965 Electrical breakdown of gases: the spatio-temporal growth of ionization in fields distorted by space charge *Proc. Roy. Soc.* **A281** 164–183

[82] Sigmond R S 1982 Simple approximate treatment of unipolar space-charge-dominated coronas: the Warburg law and the saturation current *J. Appl. Phys.* **53** 891–898

[83] Laan M, Repän V, Paris P 1998 Waveforms of UV-induced current pulses of negative corona *11th Symp. on Elementary Processes and Chemical Reactions in Low Temperature Plasma* (Low Tatras) *Contrib. Papers* **P.2** 271–273.

[84] Laan M, Aarik J, Josepson R, Repän V 2003 Low Current Mode of Negative Corona: Mechanism of Electron Emission *J. Phys. D: Appl. Phys.* **36** 2667–2672

80

[85] Repän V, Laan M, Paris P 1999 Transition to Trichel pulses for Cathodes of Different Photoelectric Yields *Proc. XXIV ICPIG'99* (Warzaw, Poland*) Contrib. Pap.* **Vol. II** 175–176

[86] Laan M 1979 Calculation of field distribution for pulses of DC corona *Acta Comment. Univ. Tartuensis* **479** 77–104 (in Russian)

[87] Simmons J G 1971 Conduction in thin dielectric films *J. Phys. D: Appl. Phys.* **4** 613–657

[88] Tang H, Prasad K, Sanjinés R and Lévy F 1995 TiO_2 anatase thin films as gas sensors *Sensors and Actuators B* **26–27** 71–75

81

ACKNOWLEDGEMENTS

PUBLICATIONS

CURRICULUM VITAE

VILLU REPÄN

Citizenship: Estonian
Date of birth: December 3, 1963
Personal status: married, 4 children
Address: Nooruse 6–1, 61001 Rõngu, Tartu county
Phone: 7 459 287
E-mail: vrepan@hot.ee

Education

1971–1979   Base School of Pedagogical School of Tartu
1979–1982   Tartu Secondary School No 10
1982–1989   University of Tartu, graduated in field of electronics
1994–1996   University of Tartu, MSc in physics
1996–2002   University of Tartu, PhD student

Professional employment

1989–1991   Rõngu experimental plant of horticultural equipment,
             engineer
1991–1993   Rõngu Tehas, engineer
1993–1995   Institute of Physics, Tartu, engineer
1996–2000   University of Tartu, EFTI, senior engineer
2000   self-employed person

ELULUGU

VILLU REPÄN

Kodakondsus: Eesti
Sünniaeg ja -koht: 3.12.1963, Türi
Perekonnaseis: abielus, 4 last
Aadress: Nooruse 6–1, 61001 Rõngu, Tartu maakond
Telefon: 7 459 287
E-post: vrepan@hot.ee

Haridus

1971–1979	Tartu Pedagoogilise Kooli Harjutuskool
1979–1982	Tartu 10. Keskkool
1982–1989	Tartu Ülikool, lõpetanud füüsik-elektroonikuna
1994–1996	Tartu Ülikool, MSc füüsikas
1996–2002	Tartu Ülikool, doktorant

Teenistuskäik

1989–1991	Rõngu Aiandusseadmete Katsetehas, insener-konstruktor
1991–1993	RAS Rõngu Tehas, elektroonikainsener
1993–1995	Füüsika Instituut, insener
1996–2000	Tartu Ülikool, EFTI, vaneminsener
2000	FIE